

Benchmarking XAI Explanations with Human-Aligned Evaluations

Rémi Kazmierczak¹, Steve Azzolin², Eloïse Berthier¹, Anna Hedström³, Patricia Delhomme⁴, David Filliat¹, Nicolas Bousquet⁵, Goran Frehse¹, Massimiliano Mancini², Baptiste Caramiaux⁶, Andrea Passerini², Gianni Franchi¹

¹Unité d'Informatique et d'Ingénierie des Systèmes, ENSTA Paris, Institut Polytechnique de Paris, Palaiseau, France

²Department of Information Engineering and Computer Science, University of Trento, Trento, Italy

³Understandable Machine Intelligence Lab, TU Berlin, Berlin, Germany

⁴Laboratory of Applied Ergonomics and Psychology, Université Gustave Eiffel, Versailles, France

⁵SINCLAIR Laboratory, Palaiseau, France

⁶Institute of Intelligent Systems and Robotics, Sorbonne Université, Paris, France

{remi.kazmierczak, eloise.berthier, goran.frehse, gianni.franchi}@ensta-paris.fr

{steve.azzolin, massimiliano.mancini, andrea.passerini}@unitn.it

hedstroem.anna@gmail.com

patricia.delhomme@univ-eiffel.fr

nicolas.bousquet@edf.fr

baptiste.caramiaux@sorbonne-universite.fr

Abstract

We introduce PASTA (Perceptual Assessment System for explanation of Artificial Intelligence), a novel human-centric framework for evaluating eXplainable AI (XAI) techniques in computer vision. Our first contribution is the creation of the **PASTA-dataset**, the first large-scale benchmark that spans a diverse set of models and both saliency-based and concept-based explanation methods. This dataset enables robust, comparative analysis of XAI techniques based on human judgment. Our second contribution is an automated, data-driven benchmark that predicts human preferences using the **PASTA-dataset**. This scoring called **PASTA-score** offers scalable, reliable, and consistent evaluation aligned with human perception. Additionally, our benchmark allows for comparisons between explanations across different modalities, an aspect previously unaddressed. We then propose to apply our scoring method to probe the interpretability of existing models and to build more human-interpretable XAI methods.

Introduction

As Deep Neural Networks (DNNs) are increasingly deployed in high-stakes domains such as law and medicine (Surden 2021; Litjens et al. 2017), understanding their decision-making process has become essential (Bender et al. 2021). Their opacity often earns them the label “black boxes” (Castelvecchi 2016), raising trust and accountability concerns in critical applications (Vereschak et al. 2024). This has given rise to the field of eXplainable AI (XAI) (Gunning et al. 2019).

A wide variety of XAI techniques have been proposed (Speith 2022; Saeed and Omlin 2023), notably saliency-based methods (Muhammad and Yeasin 2020; Böhle et al. 2024), which highlight relevant input features, and concept-based methods (Yan et al. 2023; Díaz-Rodríguez et al. 2022), which associate predictions with high-level semantic concepts. However, comparing such heterogeneous approaches

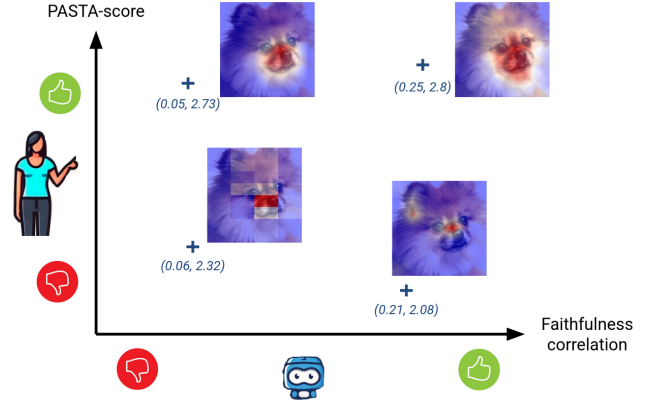


Figure 1: **PASTA automates the evaluation of human perception** of provided explanations by computing a PASTA-score. By integrating PASTA-score (y-axis) with existing faithfulness metrics (x-axis), we aim to foster the development of explanations that are not only aligned with the model’s behavior but also comprehensible to human evaluators. Samples reported in the figure correspond to the label *dog* for a ResNet50 classifier trained on PascalPART. XAI methods: top left: GradCAM; Top right: FullGrad; Bottom left: SHAP; Bottom right: AblationCAM

remains an open problem.

Evaluating XAI methods is particularly challenging for two main reasons. First, the diversity of explanation types complicates the definition of a common evaluation framework. Second, the notion of a “good explanation” is inherently subjective. This creates a dichotomy between *non-perceptual* evaluations—focused on model-centric metrics using toolkits like OpenXAI, Quantus, and Xplique (Agarwal et al. 2022b; Hedström et al. 2023; Fel et al.

2022a)—and *perceptual* evaluations, which assess human understanding. While the latter is often explored through anecdotal examples (Selvaraju et al. 2017; Wang et al. 2020), user studies (Dawoud et al. 2023; Colin et al. 2022), or region-of-interest alignment (Liu et al. 2024a; Arras, Osman, and Samek 2022), there is still a lack of standardization in assessing explanations from the human perspective (Nauta et al. 2023). Yet, this dimension is crucial—explanations faithful to the model’s reasoning may still be unintelligible to human users, limiting their actionability. In this sense, our proposed PASTA-score allows for evaluating explanations based on a combination of faithfulness and human preferences, as shown in Figure 1.

To address these challenges, we propose **PASTA**—the *Perceptual Assessment System for explanaTION of Artificial intelligence*—which aims to automate the human-aligned evaluation of XAI methods. PASTA has two core components. First, a benchmark, **PASTA-dataset**, composed of four diverse image-based classification datasets with aligned concept annotations, enabling the comparison of 20 XAI techniques across multiple architectures. Second, the **PASTA-score**, a data-driven metric designed to predict human preferences, providing a scalable way to evaluate explanations from a perceptual standpoint. Unlike prior benchmarks focused solely on saliency or user studies (Colin et al. 2022; Dawoud et al. 2023), PASTA unifies both saliency-based and concept-based methods under a single evaluation framework.

Our contributions are: (1) **Comprehensive XAI Benchmark**: We introduce the PASTA-dataset, enabling the evaluation of both visual and concept-based explanations. (2) **Large-scale Method Evaluation**: We assess 20 XAI methods across multiple datasets and models, including both post-hoc and ante-hoc methods. Our first result suggests that human annotators tend to prefer saliency and perturbation-based techniques, like LIME and SHAP. (3) **Human-aligned Explanation Scoring**: We propose **PASTA-score**, an automated yet perceptually grounded assessment of explanations, trained on the PASTA-dataset to replicate human preferences. (4) **Practical Applications**: We present three use cases of PASTA-score, showing how it can guide the design of more interpretable models, and serve as a proxy for visual human assessment in practical deployments. The pipeline of the global workflow is presented in Figure 2.

The complete PASTA framework (code, annotation, and models) will be released upon acceptance.

Related Work

Explainable AI. To address the challenge of explaining DNNs, several specialized tools have been proposed, often categorized into *post-hoc* and *ante-hoc* methods (Arrieta et al. 2020; Rudin et al. 2022). *Post-hoc* methods encompass any tool external to the model, allowing us to gain insights from any pre-trained DNN. Popular examples are GradCAM (Selvaraju et al. 2017), LIME (Ribeiro, Singh, and Guestrin 2016), and SHAP (Lundberg and Lee 2017). While most post-hoc explainers agree in providing input regions most responsible for a certain prediction, they differ in many non-trivial details, and selecting and evaluating the

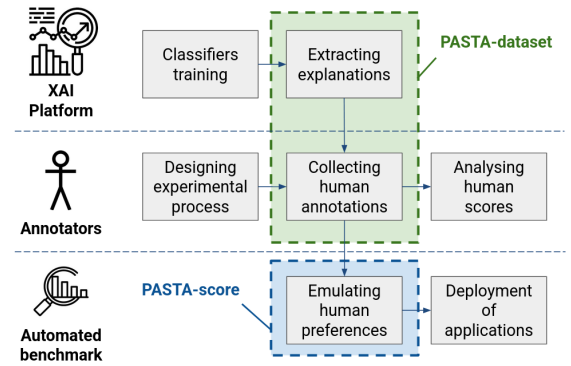


Figure 2: **Pipeline of the PASTA framework.** We first collect a dataset of human preferences called PASTA-dataset. This dataset is used to learn to emulate human preferences for the new samples on the test set using the PASTA-score. The trained PASTA-score can then be deployed to downstream applications as a consistent-over-time, quick and cost-effective replacement for human feedback.

most appropriate explainer for each task can be challenging (Leavitt and Morcos 2020; Roy et al. 2022). *Ante-hoc* methods, instead, aim at modifying the underlying model architecture to provide explanations by design. This can be done in the framework of Concept Bottleneck Models (CBMs) (Koh et al. 2020) by prompting the model to first predict a set of human-understandable high-level concepts, and then making the final prediction using a shallow and interpretable classifier that supports human inspection, or by decomposing the *reasoning* of the model into smaller and more actionable steps (Ge et al. 2023).

Evaluating explainability. While several methods have been proposed to quantitatively measure explanation quality, such as faithfulness (Petsiuk, Das, and Saenko 2018; Dasgupta, Frost, and Moshkovitz 2022; Azzolin et al. 2025), sparsity (Chalasani et al. 2020; Bénard et al. 2021), robustness (Alvarez-Melis and Jaakkola 2018b; Montavon, Samek, and Müller 2018), sensitivity (Adebayo et al. 2018; Hedström et al. 2024) and alignment to an assumed ground truth (Colin et al. 2022; Mohseni, Block, and Ragan 2021; Dawoud et al. 2023), they inherently overlook the perceptual aspect with respect to the human, who is the expected consumer of such explanations. Evaluating explanations via user studies, e.g., where annotators are asked to rate and evaluate explanations (Chen et al. 2018; Shu et al. 2019; Yang et al. 2022; Kares et al. 2025), are, however, very costly, prone to unreproducibility issues (Nauta et al. 2023), and often unfeasible for tasks that require trained users, like in the medical domain (Miró-Nicolau, Moyà-Alcover, and Jaume-i Capó 2022; Muddamsetty, Jahromi, and Moeslund 2021). In this work, we take the first step towards standardizing the evaluation of human perception preferences of explanations (Nauta et al. 2023). We propose to overcome the issues of hard-to-reproduce large-scale user studies by automating the evaluation of XAI techniques through a multi-value scoring method that mimics human preferences while

taking into account the users’ diverse expectations, which naturally emerge in user-based studies.

Automated scoring. Automated scoring involves developing models that assign scores to inputs based on a reference dataset, often derived from human ratings. A particularly active area of research in this domain is automated essay scoring. Traditionally, this has been addressed through handcrafted feature extraction (Yannakoudakis, Briscoe, and Medlock 2011), but modern methods tend to be closer to model as a judge (Lee et al. 2024; Taghipour and Ng 2016; Chiang et al. 2024). More recently, there has been a growing interest in using embeddings from large language models (LLMs) as features for scoring. The first successful attempt in this direction was made by Yang et al. (2020). Building on this trend, other approaches have incorporated LLM embeddings with models like LSTMs (Wang et al. 2022), integrated text generation into the training loop (Xiao et al. 2024), or introduced multi-scale aspects to enhance performance (Li et al. 2023).

Creating the PASTA-dataset

To assess the quality of XAI explanations for image classification decisions from a human-centric perspective, we constructed a comprehensive dataset comprising images, predictions, explanations, and evaluations of these explanations, as depicted in Figure 3. To account for the heterogeneity of different XAI methods, model backbones, and training scenarios, we constructed the PASTA-benchmark to include 1000 images sampled across 4 available datasets, 7 classification backbones, 20 XAI methods, 6 questions, and 5 annotations per image. The challenge in annotating such a dataset resides in its multiplicative nature, where each question requires an annotation across multiple backbones, datasets, XAI methods, images, and human annotators. Consequently, the PASTA-dataset contains an overall number of 633,000 samples, each corresponding to a unique Likert-like rating, which is the largest benchmark available of this kind.

To construct such a dataset, the initial phase involved developing a unified platform designed to integrate various models, XAI methods, and datasets in a streamlined manner. This platform encompasses a diverse array of models and XAI methods. Given the potential utility of this platform as a baseline for future research, we intend to release it publicly upon publication of this paper. Further details regarding the overall procedure, including details about the datasets employed, model training, and explanation extraction, are available in Section A.1 of the appendix. The subsequent phase in dataset creation is dedicated to annotating the explanations, which involved 24 participants in an online process. A pivotal insight from existing user study literature (Xuan et al. 2025; Liao et al. 2022) is that human perception of explanations is not unidimensional; rather, it encompasses a range of potentially unaligned desiderata. For instance, a saliency-based explanation that highlights a dog to predict a cat can be entirely clear, thereby satisfying complexity desiderata, while simultaneously not fulfilling plausibility desiderata. Consequently, we pose multiple questions designed to encompass a spectrum of human assessment as broad as pos-

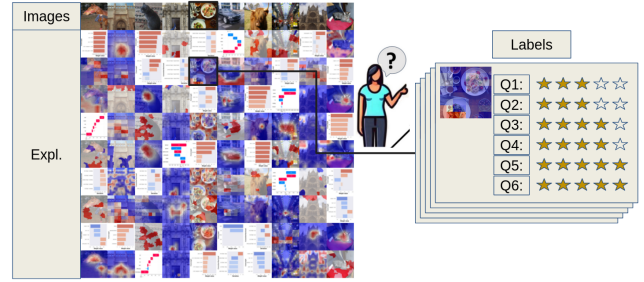


Figure 3: Overview of the human annotation process in the PASTA-dataset. We compute a total number of 46 explanations for each image, out of which 21 are sampled and rated by humans according to six questions. Further details available in Appendix A.2.

sible. Specifically, the following questions were asked:

- Q1: Is the provided explanation consistent with how I would explain the predicted class?
- Q2: Overall the explanation provided for the model prediction can be trusted?
- Q3: Is the explanation easy to understand?
- Q4: Can the explanation be understood by a large number of people, independently of their demographics (age, gender, country, etc.) and culture?
- Q5: With this perturbed image, to what extent has the explanation changed? (Examples with good predictions and light perturbations)
- Q6: With this perturbed image, to what extent has the explanation changed? (Examples with bad predictions and strong perturbations)

The selection of these questions reflects a broader discourse on user studies and desiderata. To ensure that annotators comprehensively understand the task and expectations, we implemented an evaluation protocol developed with the assistance of a psychologist. This protocol includes annotator training and continuous monitoring throughout the process. Discussions regarding the desiderata, a detailed evaluation protocol, and information about the annotators are available in Section A.2 of the Appendix.

Analysis of Human Preference

Having collected a large number of human preferences for different XAI models and backbones in the PASTA-dataset, we now proceed to analyze human scores in relation to each method. The full analysis is available in Appendix B.3.

Human preferences for output format: As illustrated in Figure 4, results indicate that humans tend to prefer image-based explainers in relation to questions Q1-Q5, meaning that saliency maps are perceived as more interpretable than concept-based explanations. Although several factors may contribute to this behavior—such as the lower cognitive load of image-based explanations compared to concept-based ones—a comprehensive investigation of the underlying psychological causes is left for future work. The sole exception

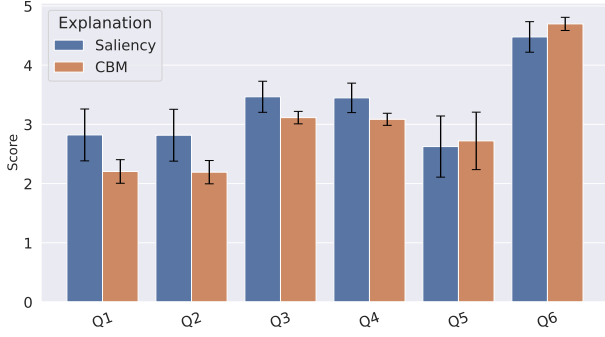


Figure 4: **Scores for each question, for saliency-based and CBM-based explanation.** Overall, saliency-based explanations are preferred over CBM-based ones.

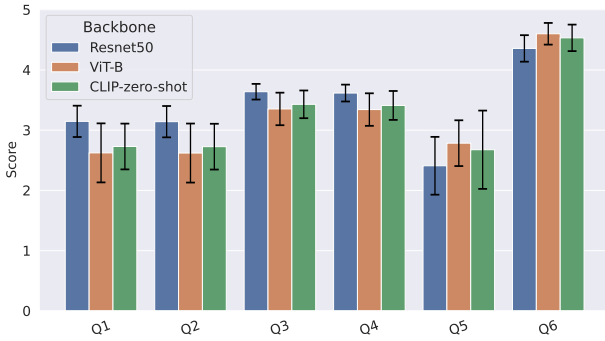


Figure 5: **Scores for each question, for different backbones of saliency methods.** As backbones for saliency methods, ViT-B and CLIP obtain overall similar results, while ResNet50 has generally better scores.

to this observation pertains to Q6 (note that for Q5, the ratings are inverted, with a low score indicating favorable behavior). This phenomenon can be explained by the fact that presenting explanations as a heatmap overlaid on the image reduces the perceptual impact of perturbations.

Human preferences for model architecture: Figure 5 illustrates the average scores across XAI methods that use the same backbone, highlighting a general preference for ResNet50. CLIP and ViT achieve similar scores, likely due to the architectural similarities between the two models. ResNet50, which played a pivotal role in the development of many XAI methods, consistently scores higher. This could suggest a potential bias toward ResNet50 in the design and effectiveness of current XAI methods. The results for the last two questions may be due to ViT being more sensitive to the perturbations used than Resnet50. Among the methods we studied, those based on feature factorization—like Eigen-CAM (Muhammad and Yeasin 2020) and Deep Feature Factorization (Collins, Achanta, and Susstrunk 2018)—tend to give more consistent and preferred explanations. This may be because they remove complex components that can create confusing artifacts, making the explanations easier to understand.

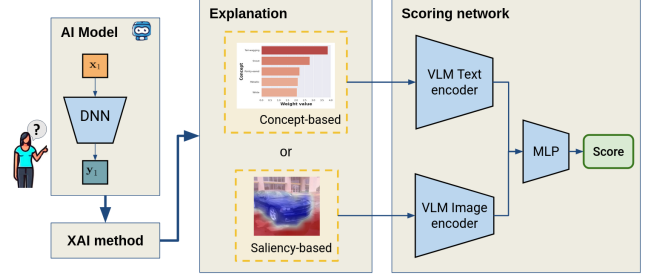


Figure 6: **Functioning of the PASTA-score.** First, we extract the embeddings for each explanation using a frozen image encoder of a VLM. Then, we employ a scoring network trained on the labels provided by the PASTA-dataset to generate a final score.

Developing the PASTA-score

To provide a tool for measuring human assessment of XAI techniques, we introduce the PASTA-score, which simulates a human evaluation. The global pipeline is illustrated in Figure 6. More precisely, the PASTA-score is composed of an embedding network, that processes both CBM outputs or saliency maps, and a scoring network, that computes scores from the embeddings. Using the data collected in the PASTA-dataset, the PASTA-score aims at predicting the human scores for questions Q1 to Q6 for new explanations, playing the role of an automated benchmark.

Computation of the embeddings

Drawing inspiration from recent literature in automated essay scoring (Yang et al. 2020; Wang et al. 2022), which encounters similar challenges due to working with a dataset of thousands of samples (21,110 samples per question, precisely) and requiring a DNN to automatically learn the score, we opt for a foundation model that we will fine-tune using a multi-linear perceptron. However, unlike automated essay scoring, we deal with both image and textual inputs, making the use of a Vision Language Model (VLM) mandatory. We tested multiple candidates, such as CLIP (Yan et al. 2023), BLIP (Li et al. 2022a) and LLaVa (Liu et al. 2024b). This choice allows for a unified integration of both concept-based explanations, which can be transformed into text, and saliency map-based explanations, which can be projected into the same embedding space. Let $x_i \in \mathbb{R}^{H \times W \times 3}$ be the i -th test image with height H and width W , and let $e_i^{saliency} \in \mathbb{R}^{H \times W}$ be a saliency-based explanation for this image. We denote the image encoder of a Vision-Language Model (VLM) as $\text{VLM}_{\text{image}}$. To embed a saliency explanation, we apply the encoder to the image overlaid with its heatmap:

$$\phi_{\text{image}}(e_i^{saliency}) = \text{VLM}_{\text{image}}(\text{Heatmap}(x_i, e_i^{saliency})), \quad (1)$$

where Heatmap generates the visual overlay of the explanation on the image.

For concept-based methods (CBMs), let $e_i^{CBM} \in \mathbb{R}^K$ be the explanation vector, where K is the number of concepts.

This vector is turned into a sentence using a text template, and then encoded with the VLM’s text encoder VLM_{text} :

$$\phi_{\text{text}}(e_i^{CBM}) = VLM_{\text{text}}(\text{Sentence}(e_i^{CBM})). \quad (2)$$

Since the PASTA-score is compatible with different VLMs and does not rely on a specific one, we evaluate it using several VLMs: CLIP (Liu et al. 2024b), SIGLIP (Zhai et al. 2023), EVA (Sun et al. 2023), and BLIP (Li et al. 2022a). This results in multiple variants of our metric: PASTA-score^{CLIP}, PASTA-score^{SIGLIP}, PASTA-score^{EVA}, and PASTA-score^{BLIP}.

To support our design choices, Appendix D.2 presents extensive ablations on various factors: the impact of textual templates, the number of concepts K , the way saliency maps are visualized, and whether label information is included. We also explore alternative versions of Equations 1 and 2, and how these choices affect the final score.

Scoring network

Once the embeddings are computed, the label information is concatenated to the embedding, and a scoring network composed of a multi-layer perceptron is used to predict scores. Inspired by Automated Essay Scoring (Yang et al. 2020; Wang et al. 2022), we use a loss L that combines a similarity loss L_s , a mean squared error (MSE) loss L_{mse} , and a ranking loss L_r . From a set of ground truth scores obtained from majority voting $\{m_k\}_{k \in [0, N_s]}$ and the predictions given by the scoring network $\{\hat{m}_k\}_{k \in [0, N_s]}$, the resulting loss is defined as:

$$L(m_k, \hat{m}_k) = \alpha L_s(m_k, \hat{m}_k) + \beta L_{mse}(m_k, \hat{m}_k) + \gamma L_r(m_k, \hat{m}_k), \quad (3)$$

where α , β , and γ are hyperparameters controlling the relative importance of each component. Formulas about the different losses are given in Appendix D.1. Since the PASTA dataset provides 5 ground-truth votes per inference, we explored different aggregation strategies. To mitigate the phenomenon of high non-consensus, the mode was selected as the final choice.

Classifier results

Note that in the PASTA-dataset each sample corresponds to a triplet (input image, explanation, human ratings). The same image thus appears multiple times for different XAI methods, and the same XAI method appears multiple times for different images. To guarantee that no leakage occurs between train-test splits, we design them to ensure that the same image, or the same XAI method, does not appear in different splits. Images and XAI methods included in the training splits are randomly chosen based on the run’s random seed. For Q1 to Q6, we calculate the Mean Square Error (MSE), Quadratic Weighted Kappa (QWK), and Spearman Correlation Coefficient (SCC) between the predicted and ground truth labels on the test set. The results are presented in Table 1, where we also ablate different choices of embedding methods. We also report the inter-annotator agreement values, which correspond to the expected deviation of the metrics between a randomly selected annotator’s score and

the mode. Our network best replicates answers to Q1 and Q2, with similar performance across PASTA-score^{CLIP} and PASTA-score^{SIGLIP}. This is likely due to greater rating diversity and stronger agreement between annotators, which supports more stable training. In contrast, Q3 to Q5 shows lower agreement, and Q5–Q6 has less diverse ratings. While the MSE stays similar, it becomes harder to learn the ranking patterns, likely due to the more subjective nature of these questions and the added uncertainty from image perturbations in Q5 and Q6.

Alignment with Established Benchmarks

In this subsection, we aim to evaluate whether the PASTA-score aligns with the findings of existing studies that compare human assessments of XAI methods. To accomplish this, we use the benchmark dataset established by Yang et al. (2022), which offers comparative evaluations of GradCAM (Selvaraju et al. 2017), RISE (Petsiuk, Das, and Saenko 2018) (at the image level), and Guided Backpropagation (Springenberg et al. 2014). These quantitative evaluations are presented in the form of Mean Absolute Error (MAE) between generated saliency maps and those produced by a Human Saliency Imitator (HSI). Given that this benchmark aims to explore human expectations, we compare the results obtained by the authors (MAE) with the PASTA-score related to Q1.

The results are summarized in Table 2, and indicate that despite RISE and Guided Backpropagation not being included during the training of the PASTA metric, the obtained rankings remain consistent. This provides empirical evidence supporting the generalization of the PASTA-score to unseen XAI techniques.

Applications

In this section, we explore three different applications using the PASTA-score as a replacement for human feedback, which would be difficult or too costly to run at scale without automation. We use PASTA-score to guide XAI methods toward better interpretability (in the first and third applications) and to analyze how model size affects interpretability (in the second application). All experiments use the PASTA-score model trained on Q1 for consistency.

Mixture of XAI methods

Our first application is to dynamically select the explainer giving the explanation that best matches human judgments for each specific image, using a mixture of XAI methods. In our experiments, we fix the classifier to be a ResNet50, and we select the explanation with the highest PASTA-score for each image. The distribution of selected XAI methods is shown in Table 7. The results indicate a substantial diversity in the methods employed, with FullGrad emerging as the most frequently used, selected nearly half of the time. This trend is reflective of user ratings within the PASTA-dataset, where FullGrad is identified as providing the most effective explanations according to annotators. In terms of faithfulness, the computation of the average faithfulness correlation across explanations selected by our PASTA-score

Table 1: **Mean Square Error (MSE), Quadratic Weighted Kappa (QWK), and Spearman Correlation Coefficient (SCC) for each question.** Each value is the average of 5 runs with standard deviation. *Human* refers to inter-annotator agreement.

Metric	Model	Q1	Q2	Q3	Q4	Q5	Q6
MSE ↓	PASTA-score ^{CLIP}	0.990 ± 0.104	0.993 ± 0.096	2.111 ± 2.529	0.811 ± 0.095	1.476 ± 0.183	0.752 ± 0.127
	PASTA-score ^{SIGLIP}	0.989 ± 0.113	1.009 ± 0.125	0.842 ± 0.094	0.840 ± 0.106	1.396 ± 0.177	0.739 ± 0.140
	PASTA-score ^{BLIP}	3.297 ± 1.840	3.287 ± 1.835	5.938 ± 2.542	4.642 ± 3.135	3.005 ± 1.385	10.710 ± 4.943
	PASTA-score ^{EVA}	1.666 ± 1.215	1.747 ± 1.174	3.355 ± 3.099	2.097 ± 2.608	1.767 ± 0.568	3.324 ± 5.091
	<i>Human</i>	0.415 ± 0.037	0.429 ± 0.049	0.562 ± 0.104	0.478 ± 0.080	0.509 ± 0.102	0.299 ± 0.051
QWK ↑	PASTA-score ^{CLIP}	0.450 ± 0.066	0.452 ± 0.063	0.199 ± 0.040	0.216 ± 0.052	0.165 ± 0.060	0.159 ± 0.031
	PASTA-score ^{SIGLIP}	0.471 ± 0.055	0.459 ± 0.056	0.237 ± 0.052	0.219 ± 0.035	0.177 ± 0.061	0.165 ± 0.018
	PASTA-score ^{BLIP}	0.328 ± 0.023	0.340 ± 0.020	0.181 ± 0.003	0.173 ± 0.017	0.081 ± 0.081	0.159 ± 0.011
	PASTA-score ^{EVA}	0.462 ± 0.050	0.457 ± 0.054	0.160 ± 0.099	0.230 ± 0.018	0.163 ± 0.029	0.185 ± 0.049
	<i>Human</i>	0.849 ± 0.013	0.845 ± 0.017	0.731 ± 0.050	0.748 ± 0.041	0.848 ± 0.029	0.796 ± 0.048
SCC ↑	PASTA-score ^{CLIP}	0.484 ± 0.064	0.484 ± 0.062	0.213 ± 0.040	0.230 ± 0.050	0.197 ± 0.073	0.193 ± 0.030
	PASTA-score ^{SIGLIP}	0.501 ± 0.052	0.490 ± 0.057	0.247 ± 0.048	0.223 ± 0.029	0.213 ± 0.071	0.196 ± 0.020
	PASTA-score ^{BLIP}	0.397 ± 0.036	0.411 ± 0.033	0.207 ± 0.065	0.194 ± 0.014	0.088 ± 0.104	0.218 ± 0.012
	PASTA-score ^{EVA}	0.484 ± 0.046	0.474 ± 0.048	0.150 ± 0.155	0.247 ± 0.015	0.216 ± 0.035	0.220 ± 0.057
	<i>Human</i>	0.844 ± 0.017	0.839 ± 0.019	0.722 ± 0.045	0.742 ± 0.038	0.850 ± 0.023	0.789 ± 0.039

Table 2: **Comparison of Rankings Based on HSI and PASTA-Scores.** The results illustrate that the PASTA-score exhibits a correlation with the Human Saliency Imitator presented by (Yang et al. 2022).

Method	MAE Score ↓	PASTA-score ↑
RISE	0.442	3.113
GradCAM	0.703	3.150
Guided Backpropagation	0.890	1.846

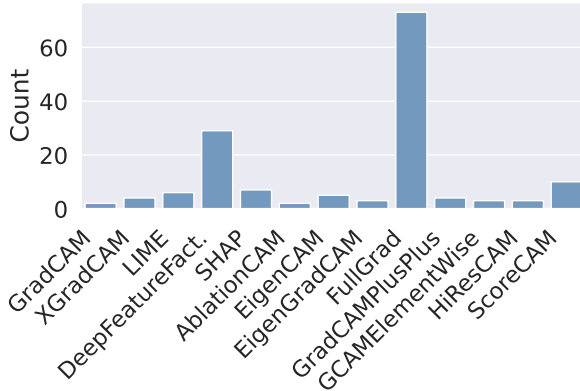
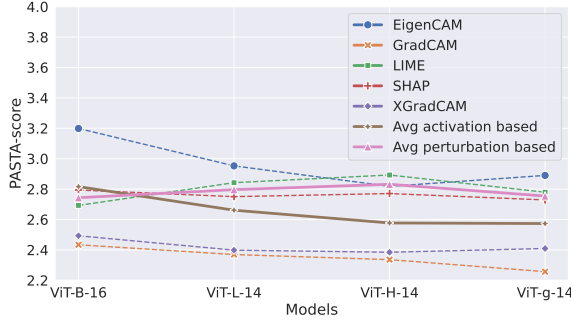


Figure 7: **Distribution of methods selected by our mixture of XAI techniques.** The x-axis denotes the number of images in the automated benchmark for which the respective XAI method attained the highest performance.

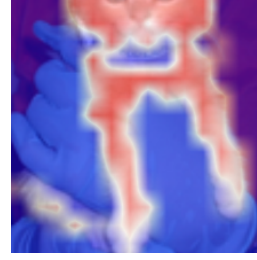
yields a relatively stable value, with a slight improvement compared to the value obtained by averaging over every explainer (0.0627 for our selection versus 0.0579 for the average over every explainer). This confirms that it is possible to use PASTA to enhance the interpretability of explanations without compromising their faithfulness.

Backbone size influence on the understanding of explanation

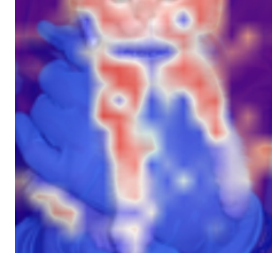
We use the PASTA-score to investigate whether model size influences the human perception of explanations, and how this relates to XAI methods. To this end, we compute the average PASTA-score within an identical experimental framework, varying only the size of the backbone model. Specifically, we employ CLIP as the classifier and select backbones from among its ViT-B-16, ViT-L-14, ViT-H-14, and ViT-g-14 variants. The results of this analysis are presented in Figure 8. Our results show that for activation map-based XAI methods, performance metrics drop as the model size increases. This decline is particularly pronounced when transitioning from the ViT-B to the ViT-L architecture. Several hypotheses may account for this phenomenon. The most plausible explanation is the emergence of artifacts associated with high-norm tokens in the activation maps of larger models, which are used to store information (Darcet et al. 2023). Interestingly, this decrease in score is not percepti-



(a) Comparison of various XAI methods across different ViT models.



(b) ViT-B-16; PASTA-score of the explanation: 3.12



(c) ViT-g-14; PASTA-score of the explanation: 2.75

Figure 8: Impact of classifier backbone size on the perceived interpretability of image explanations. A notable decrease in the PASTA-score is observed as the model size increases (left). Examination of image samples suggests that artifacts present in the background are likely responsible for this decline.

ble in image perturbation-based XAI techniques, which reinforces the hypothesis that activation artifacts contribute to the reduced interpretability of explanations.

Steering XAI methods towards better alignment

We propose to use the PASTA-score to enhance the interpretability of an off-the-shelf XAI method, namely RISE (Petsiuk, Das, and Saenko 2018). Our approach is as follows: while RISE generates random masks and selects the one that has the best class scores S_{proba} , we introduce a regularization component based on the PASTA-score. Consequently, instead of rating masks using S_{proba} , we employ the following formula:

$$w_{RISE+PASTA} = \lambda S_{PASTA} + (1 - \lambda) S_{proba}, \quad (4)$$

where $\lambda \in [0, 1]$ is a hyperparameter. When $\lambda = 0$, the generated explanation aligns with the original RISE method. Conversely, if $\lambda = 1$, the explanation produced corresponds to a scenario that maximizes the PASTA-score. Note that setting $\lambda = 1$ would result in an explainer optimizing only for human preferences while neglecting the true behavior of the model, which may not yield useful explanations.

Upon analyzing the samples generated through the optimization process, we initially observe a slight improvement in the localization of highlighted objects. For instance, the explanation depicted in Figure 9e exhibits fewer indecisive zones and demonstrates enhanced precision compared to the explanation shown in Figure 9d. Regarding the case where $\lambda = 1$, we note that the explanation begins to hallucinate zones of interest while omitting others, like in Figure 9c. Additionally, one can observe that the PASTA-score favors large heatmaps. However, the optimized explanations do not systematically overlap with the entire zone of the prediction, suggesting that alignment with the segmentation map of the object to assess the quality of saliency-based explanations, as conducted in previous studies (Karmani et al. 2024; Li et al. 2022b), may prove to be inadequate.



(a) $\lambda = 0$
 $F = 0.0983$
 $P = 4.13$



(b) $\lambda = 0.7$
 $F = 0.0874$
 $P = 4.19$



(c) $\lambda = 1$
 $F = 0.0326$
 $P = 4.32$



(d) $\lambda = 0$
 $F = 0.0692$
 $P = 2.82$



(e) $\lambda = 0.7$
 $F = 0.0731$
 $P = 2.96$



(f) $\lambda = 1$
 $F = 0.0674$
 $P = 3.15$

Figure 9: Optimized explanations derived through RISE adjusted with the PASTA-score. Label of the top images: home_or_hotel. Label of the bottom images: Renaissance. F denotes the faithfulness correlation score, P denotes the PASTA-score.

Conclusions

We introduce PASTA, a novel perceptual scoring method designed to benchmark XAI techniques in a human-centric manner. We collect a large-scale benchmark dataset (PASTA-dataset), and use it for an assessment of XAI explanations by human annotators. Based on this dataset, we develop an automated scoring method (PASTA-score) that spans previously unexplored modalities, effectively mimicking human preferences and allowing for circumventing resource-intensive user studies for applications that may benefit so. Deploying PASTA allows new quantitative ob-

servations: Our findings reveal a distinct preference for saliency-based explanations, identify a negative impact of backbone size, and demonstrate the potential to generate more human pleasant explanations without compromising faithfulness. These results not only align with human intuition but also corroborate visual examples, affirming the scalability and reliability of PASTA-score.

Limitations: First, the PASTA-score is trained on specific datasets and explanation modalities, which may limit its generalizability to other unseen domains, especially those with domain-specific semantics. Second, the human preferences captured by the PASTA-dataset may inherit the intrinsic biases of human annotators. Third, although PASTA reduces the need for costly user studies, it remains an approximation of subjective human judgment and may overlook nuanced or task-specific interpretability needs, which may justify the need for more resource-intensive ad-hoc human interactions in downstream use cases.

Broader impact: Dynamic scoring approaches could be explored to capture the evolving nature of XAI techniques and their use in real-world applications. PASTA intends to take a step towards creating a transparent and trustworthy AI ecosystem. By aligning AI explanations with human preferences, we aim to foster the development of more interpretable AI systems that can be understood and trusted by users. This work also introduces a perceptual metric, paving the way for future research to implement the PASTA-score as a perceptual loss aimed at enhancing the trustworthiness of networks, drawing for example, inspiration from the emerging use of LPIPS (Zhang et al. 2018) in tasks such as image generation (Jo, Yang, and Kim 2020).

Acknowledgements

This work was performed using HPC resources from GENCI-IDRIS (Grant 2024 - AD011014675R1).

References

- Adebayo, J.; Gilmer, J.; Muelly, M.; Goodfellow, I. J.; Hardt, M.; and Kim, B. 2018. Sanity Checks for Saliency Maps. In Bengio, S.; Wallach, H. M.; Larochelle, H.; Grauman, K.; Cesa-Bianchi, N.; and Garnett, R., eds., *Advances in Neural Information Processing Systems 31: Annual Conference on Neural Information Processing Systems 2018, NeurIPS 2018, December 3-8, 2018, Montréal, Canada*, 9525–9536.
- Agarwal, C.; Johnson, N.; Pawelczyk, M.; Krishna, S.; Saxena, E.; Zitnik, M.; and Lakkaraju, H. 2022a. Rethinking stability for attribution-based explanations. *arXiv preprint arXiv:2203.06877*.
- Agarwal, C.; Krishna, S.; Saxena, E.; Pawelczyk, M.; Johnson, N.; Puri, I.; Zitnik, M.; and Lakkaraju, H. 2022b. Openxai: Towards a transparent evaluation of model explanations. *Advances in Neural Information Processing Systems*, 35: 15784–15799.
- Alvarez-Melis, D.; and Jaakkola, T. 2018a. Towards robust interpretability with self-explaining neural networks. *Advances in Neural Information Processing Systems*, 31.
- Alvarez-Melis, D.; and Jaakkola, T. S. 2018b. On the robustness of interpretability methods. *arXiv preprint arXiv:1806.08049*.
- Ancona, M.; Ceolini, E.; Öztireli, C.; and Gross, M. 2017. Towards better understanding of gradient-based attribution methods for deep neural networks. *arXiv preprint arXiv:1711.06104*.
- Arras, L.; Osman, A.; and Samek, W. 2022. CLEVR-XAI: A benchmark dataset for the ground truth evaluation of neural network explanations. *Information Fusion*, 81: 14–40.
- Arrieta, A. B.; Díaz-Rodríguez, N.; Del Ser, J.; Bennetot, A.; Tabik, S.; Barbado, A.; García, S.; Gil-López, S.; Molina, D.; Benjamins, R.; et al. 2020. Explainable Artificial Intelligence (XAI): Concepts, taxonomies, opportunities and challenges toward responsible AI. *Information Fusion*, 58: 82–115.
- Arya, V.; Bellamy, R. K.; Chen, P.-Y.; Dhurandhar, A.; Hind, M.; Hoffman, S. C.; Houde, S.; Liao, Q. V.; Luss, R.; Mojsilović, A.; et al. 2019. One explanation does not fit all: A toolkit and taxonomy of ai explainability techniques. *arXiv preprint arXiv:1909.03012*.
- Azzolin, S.; Longa, A.; Teso, S.; and Passerini, A. 2025. Reconsidering Faithfulness in Regular, Self-Explainable and Domain Invariant GNNs. In *The Thirteenth International Conference on Learning Representations*.
- Bach, S.; Binder, A.; Montavon, G.; Klauschen, F.; Müller, K.-R.; and Samek, W. 2015. On pixel-wise explanations for non-linear classifier decisions by layer-wise relevance propagation. *PLoS One*, 10(7): e0130140.
- Bénard, C.; Biau, G.; Da Veiga, S.; and Scornet, E. 2021. Interpretable random forests via rule extraction. In *International Conference on Artificial Intelligence and Statistics*, 937–945.
- Bender, E. M.; Gebru, T.; McMillan-Major, A.; and Shmitchell, S. 2021. On the dangers of stochastic parrots: Can language models be too big? In *Proceedings of the 2021 ACM conference on fairness, accountability, and transparency*, 610–623.
- Bennetot, A.; Franchi, G.; Del Ser, J.; Chatila, R.; and Diaz-Rodriguez, N. 2022. Greybox XAI: A Neural-Symbolic learning framework to produce interpretable predictions for image classification. *Knowledge-Based Systems*, 258: 109947.
- Bhatt, U.; Weller, A.; and Moura, J. M. F. 2021. Evaluating and aggregating feature-based model explanations. In *Proceedings of the Twenty-Ninth International Joint Conference on Artificial Intelligence, IJCAI’20*.
- Biessmann, F.; and Refiano, D. 2021. Quality metrics for transparent machine learning with and without humans in the loop are not correlated. *arXiv preprint arXiv:2107.02033*.
- Böhle, M.; Singh, N.; Fritz, M.; and Schiele, B. 2024. B-cos alignment for inherently interpretable CNNs and vision transformers. *IEEE Transactions on Pattern Analysis and Machine Intelligence*, 46(6): 4504–4518.
- Castelvecchi, D. 2016. Can we open the black box of AI? *Nature News*, 538(7623): 20.

- Chalasanani, P.; Chen, J.; Chowdhury, A. R.; Wu, X.; and Jha, S. 2020. Concise explanations of neural networks using adversarial training. In *International Conference on Machine Learning*, 1383–1391.
- Chattopadhyay, A.; Sarkar, A.; Howlader, P.; and Balasubramanian, V. N. 2018. Grad-cam++: Generalized gradient-based visual explanations for deep convolutional networks. In *2018 IEEE Winter Conference on Applications of Computer Vision (WACV)*, 839–847. IEEE.
- Chen, C.; Zhang, M.; Liu, Y.; and Ma, S. 2018. Neural attentional rating regression with review-level explanations. In *Proceedings of the 2018 World Wide Web Conference*, 1583–1592.
- Chiang, W.-L.; Zheng, L.; Sheng, Y.; Angelopoulos, A. N.; Li, T.; Li, D.; Zhang, H.; Zhu, B.; Jordan, M.; Gonzalez, J. E.; and Stoica, I. 2024. Chatbot Arena: An Open Platform for Evaluating LLMs by Human Preference. *arXiv:2403.04132*.
- Colin, J.; Fel, T.; Cadène, R.; and Serre, T. 2022. What I cannot predict, I do not understand: A human-centered evaluation framework for explainability methods. *Advances in Neural Information Processing Systems*, 35: 2832–2845.
- Collins, E.; Achanta, R.; and Susstrunk, S. 2018. Deep feature factorization for concept discovery. In *Proceedings of the European Conference on Computer Vision (ECCV)*, 336–352.
- Cowan, N. 2001. The magical number 4 in short-term memory: A reconsideration of mental storage capacity. *Behavioral and Brain Sciences*, 24(1): 87–114.
- Darcet, T.; Oquab, M.; Mairal, J.; and Bojanowski, P. 2023. Vision transformers need registers. *arXiv preprint arXiv:2309.16588*.
- Dasgupta, S.; Frost, N.; and Moshkovitz, M. 2022. Framework for evaluating faithfulness of local explanations. In *International Conference on Machine Learning*, 4794–4815.
- Dawoud, K.; Samek, W.; Eisert, P.; Lapuschkin, S.; and Bosse, S. 2023. Human-Centered Evaluation of XAI Methods. In *2023 IEEE International Conference on Data Mining Workshops (ICDMW)*, 912–921. IEEE.
- Díaz-Rodríguez, N.; Lamas, A.; Sanchez, J.; Franchi, G.; Donadello, I.; Tabik, S.; Filliat, D.; Cruz, P.; Montes, R.; and Herrera, F. 2022. EXplainable Neural-Symbolic Learning (X-NeSyL) methodology to fuse deep learning representations with expert knowledge graphs: The MonuMAI cultural heritage use case. *Information Fusion*, 79: 58–83.
- Doshi-Velez, F.; and Kim, B. 2017. Towards a rigorous science of interpretable machine learning. *arXiv preprint arXiv:1702.08608*.
- Dosovitskiy, A. 2020. An image is worth 16x16 words: Transformers for image recognition at scale. *arXiv preprint arXiv:2010.11929*.
- Draeos, R. L.; and Carin, L. 2020. Use HiResCAM instead of Grad-CAM for faithful explanations of convolutional neural networks. *arXiv preprint arXiv:2011.08891*.
- Fel, T.; Hervier, L.; Vigouroux, D.; Poche, A.; Plakoo, J.; Cadene, R.; Chalvidal, M.; Colin, J.; Boissin, T.; Bethune, L.; Picard, A.; Nicodeme, C.; Gardes, L.; Flandin, G.; and Serre, T. 2022a. Xplique: A Deep Learning Explainability Toolbox. *Workshop on Explainable Artificial Intelligence for Computer Vision (CVPR)*.
- Fel, T.; Vigouroux, D.; Cadène, R.; and Serre, T. 2022b. How good is your explanation? algorithmic stability measures to assess the quality of explanations for deep neural networks. In *Proceedings of the IEEE/CVF Winter Conference on Applications of Computer Vision*, 720–730.
- Fu, R.; Hu, Q.; Dong, X.; Guo, Y.; Gao, Y.; and Li, B. 2020. Axiom-based grad-cam: Towards accurate visualization and explanation of CNNs. *arXiv preprint arXiv:2008.02312*.
- Ge, J.; Luo, H.; Qian, S.; Gan, Y.; Fu, J.; and Zhang, S. 2023. Chain of thought prompt tuning in vision language models. *arXiv preprint arXiv:2304.07919*.
- Gunning, D.; Stefik, M.; Choi, J.; Miller, T.; Stumpf, S.; and Yang, G.-Z. 2019. XAI—Explainable artificial intelligence. *Science Robotics*, 4(37): eaay7120.
- Hase, P.; Xie, H.; and Bansal, M. 2024. The out-of-distribution problem in explainability and search methods for feature importance explanations. In *Proceedings of the 35th International Conference on Neural Information Processing Systems*.
- He, K.; Zhang, X.; Ren, S.; and Sun, J. 2016. Deep residual learning for image recognition. In *Proceedings of the IEEE conference on computer vision and pattern recognition*, 770–778.
- Hedström, A.; Weber, L.; Krakowczyk, D.; Bareeva, D.; Motzkus, F.; Samek, W.; Lapuschkin, S.; and Höhne, M. M. 2023. Quantus: An Explainable AI Toolkit for Responsible Evaluation of Neural Network Explanations and Beyond. *Journal of Machine Learning Research*, 24(34): 1–11.
- Hedström, A.; Weber, L.; Lapuschkin, S.; and Höhne, M. 2024. Sanity checks revisited: An exploration to repair the model parameter randomisation test. *arXiv preprint arXiv:2401.06465*.
- Herm, L.-V.; Wanner, J.; Seubert, F.; and Janiesch, C. 2021. I Don’t Get IT, but IT seems Valid! The Connection between Explainability and Comprehensibility in (X) AI Research. In *ECIS*.
- Hurley, N.; and Rickard, S. 2009. Comparing measures of sparsity. *IEEE Transactions on Information Theory*, 55(10): 4723–4741.
- Jo, Y.; Yang, S.; and Kim, S. J. 2020. Investigating loss functions for extreme super-resolution. In *Proceedings of the IEEE/CVF conference on computer vision and pattern recognition workshops*, 424–425.
- Kares, F.; Speith, T.; Zhang, H.; and Langer, M. 2025. What Makes for a Good Saliency Map? Comparing Strategies for Evaluating Saliency Maps in Explainable AI (XAI). *arXiv preprint arXiv:2504.17023*.
- Karmani, S.; Sivakaran, T.; Prasad, G.; Ali, M.; Yang, W.; and Tang, S. 2024. KPCA-CAM: Visual Explainability of Deep Computer Vision Models using Kernel PCA. In *2024 IEEE 26th International Workshop on Multimedia Signal Processing (MMSP)*, 1–5. IEEE.

- Kazmierczak, R.; Berthier, E.; Frehse, G.; and Franchi, G. 2024. CLIP-QDA: An Explainable Concept Bottleneck Model. *Transactions on Machine Learning Research Journal*.
- Kingma, D. P.; and Ba, J. 2017. Adam: A Method for Stochastic Optimization. *arXiv:1412.6980*.
- Koh, P. W.; Nguyen, T.; Tang, Y. S.; Mussmann, S.; Pierson, E.; Kim, B.; and Liang, P. 2020. Concept bottleneck models. In *International Conference on Machine Learning*, 5338–5348.
- Leavitt, M. L.; and Morcos, A. 2020. Towards falsifiable interpretability research. *arXiv preprint arXiv:2010.12016*.
- Lee, S.; Kim, S.; Park, S. H.; Kim, G.; and Seo, M. 2024. Prometheusvision: Vision-language model as a judge for fine-grained evaluation. *arXiv preprint arXiv:2401.06591*.
- Li, F.; Xi, X.; Cui, Z.; Li, D.; and Zeng, W. 2023. Automatic essay scoring method based on multi-scale features. *Applied Sciences*, 13(11): 6775.
- Li, J.; Li, D.; Xiong, C.; and Hoi, S. 2022a. Blip: Bootstrapping language-image pre-training for unified vision-language understanding and generation. In *International conference on machine learning*, 12888–12900. PMLR.
- Li, Y.; Wang, H.; Duan, Y.; Xu, H.; and Li, X. 2022b. Exploring visual interpretability for contrastive language-image pre-training. *arXiv preprint arXiv:2209.07046*.
- Liao, Q. V.; Zhang, Y.; Luss, R.; Doshi-Velez, F.; and Dhurandhar, A. 2022. Connecting algorithmic research and usage contexts: a perspective of contextualized evaluation for explainable AI. In *Proceedings of the AAAI Conference on Human Computation and Crowdsourcing*, volume 10, 147–159.
- Lin, C.-Y. 2004. Rouge: A package for automatic evaluation of summaries. In *Text summarization branches out*, 74–81.
- Litjens, G.; Kooi, T.; Bejnordi, B. E.; Setio, A. A. A.; Ciompi, F.; Ghafoorian, M.; Van Der Laak, J. A.; Van Ginneken, B.; and Sánchez, C. I. 2017. A survey on deep learning in medical image analysis. *Medical Image Analysis*, 42: 60–88.
- Liu, G.; Zhang, J.; Chan, A. B.; and Hsiao, J. H. 2024a. Human attention guided explainable artificial intelligence for computer vision models. *Neural Networks*, 177: 106392.
- Liu, H.; Li, C.; Wu, Q.; and Lee, Y. J. 2024b. Visual instruction tuning. *Advances in neural information processing systems*, 36.
- Liu, S.; Zeng, Z.; Ren, T.; Li, F.; Zhang, H.; Yang, J.; Li, C.; Yang, J.; Su, H.; Zhu, J.; et al. 2023. Grounding dino: Marrying dino with grounded pre-training for open-set object detection. *arXiv preprint arXiv:2303.05499*.
- Lundberg, S. M.; and Lee, S.-I. 2017. A unified approach to interpreting model predictions. *Advances in Neural Information Processing Systems*, 30.
- Miró-Nicolau, M.; Moyà-Alcover, G.; and Jaume-i Capó, A. 2022. Evaluating explainable artificial intelligence for x-ray image analysis. *Applied Sciences*, 12(9): 4459.
- Mohseni, S.; Block, J. E.; and Ragan, E. 2021. Quantitative evaluation of machine learning explanations: A human-grounded benchmark. In *26th International Conference on Intelligent User Interfaces*, 22–31.
- Montavon, G.; Samek, W.; and Müller, K.-R. 2018. Methods for interpreting and understanding deep neural networks. *Digital Signal Processing*, 73: 1–15.
- Morrison, K.; Jain, M.; Hammer, J.; and Perer, A. 2023. Eye into AI: Evaluating the interpretability of explainable AI techniques through a game with a purpose. *Proceedings of the ACM on Human-Computer Interaction*, 7(CSCW2): 1–22.
- Muddamsetty, S. M.; Jahromi, M. N.; and Moeslund, T. B. 2021. Expert level evaluations for explainable AI (XAI) methods in the medical domain. In *International Conference on Pattern Recognition*, 35–46. Springer.
- Muhammad, M. B.; and Yeasin, M. 2020. Eigen-cam: Class activation map using principal components. In *2020 International Joint Conference on Neural Networks (IJCNN)*, 1–7. IEEE.
- Nauta, M.; Trienes, J.; Pathak, S.; Nguyen, E.; Peters, M.; Schmitt, Y.; Schlötterer, J.; van Keulen, M.; and Seifert, C. 2023. From anecdotal evidence to quantitative evaluation methods: A systematic review on evaluating explainable AI. *ACM Computing Surveys*, 55(13s): 1–42.
- Nguyen, A.-p.; and Martínez, M. R. 2020. On quantitative aspects of model interpretability. *arXiv preprint arXiv:2007.07584*.
- Papineni, K.; Roukos, S.; Ward, T.; and Zhu, W.-J. 2002. Bleu: a method for automatic evaluation of machine translation. In *Proceedings of the 40th annual meeting of the Association for Computational Linguistics*, 311–318.
- Petsiuk, V.; Das, A.; and Saenko, K. 2018. Rise: Randomized input sampling for explanation of black-box models. *arXiv preprint arXiv:1806.07421*.
- Pillai, V.; and Pirsiavash, H. 2021. Explainable models with consistent interpretations. In *Proceedings of the AAAI Conference on Artificial Intelligence*, volume 35, 2431–2439.
- Pommeranz, A.; Broekens, J.; Wiggers, P.; Brinkman, W.-P.; and Jonker, C. M. 2012. Designing interfaces for explicit preference elicitation: a user-centered investigation of preference representation and elicitation process. *User Modeling and User-Adapted Interaction*, 22: 357–397.
- Radford, A.; Kim, J. W.; Hallacy, C.; Ramesh, A.; Goh, G.; Agarwal, S.; Sastry, G.; Askell, A.; Mishkin, P.; Clark, J.; et al. 2021. Learning transferable visual models from natural language supervision. In *International Conference on Machine Learning*, 8748–8763.
- Ramaswamy, H. G.; et al. 2020. Ablation-cam: Visual explanations for deep convolutional network via gradient-free localization. In *Proceedings of the IEEE/CVF Winter Conference on Applications of Computer Vision*, 983–991.
- Ribeiro, M. T.; Singh, S.; and Guestrin, C. 2016. “Why Should I Trust You?”: Explaining the Predictions of Any Classifier. In *Proceedings of the 22nd ACM SIGKDD International Conference on Knowledge Discovery and Data*

- Mining, San Francisco, CA, USA, August 13-17, 2016, 1135–1144.
- Rieger, L.; and Hansen, L. K. 2020. Irof: a low resource evaluation metric for explanation methods. *arXiv preprint arXiv:2003.08747*.
- Rong, Y.; Leemann, T.; Borisov, V.; Kasneci, G.; and Kasneci, E. 2022. A consistent and efficient evaluation strategy for attribution methods. *arXiv preprint arXiv:2202.00449*.
- Roy, S.; Laberge, G.; Roy, B.; Khomh, F.; Nikanjam, A.; and Mondal, S. 2022. Why don't XAI techniques agree? Characterizing the disagreements between post-hoc explanations of defect predictions. In *2022 IEEE International Conference on Software Maintenance and Evolution (ICSME)*, 444–448. IEEE.
- Rudin, C.; Chen, C.; Chen, Z.; Huang, H.; Semenova, L.; and Zhong, C. 2022. Interpretable machine learning: Fundamental principles and 10 grand challenges. *Statistic Surveys*, 16: 1–85.
- Saeed, W.; and Omlin, C. 2023. Explainable AI (XAI): A systematic meta-survey of current challenges and future opportunities. *Knowledge-Based Systems*, 263: 110273.
- Samek, W.; Binder, A.; Montavon, G.; Lapuschkin, S.; and Müller, K.-R. 2016. Evaluating the visualization of what a deep neural network has learned. *IEEE Transactions on Neural Networks and Learning Systems*, 28(11): 2660–2673.
- Selvaraju, R. R.; Cogswell, M.; Das, A.; Vedantam, R.; Parikh, D.; and Batra, D. 2017. Grad-cam: Visual explanations from deep networks via gradient-based localization. In *Proceedings of the IEEE International Conference on Computer Vision*, 618–626.
- Shu, K.; Cui, L.; Wang, S.; Lee, D.; and Liu, H. 2019. defend: Explainable fake news detection. In *Proceedings of the 25th ACM SIGKDD International Conference on Knowledge Discovery & Data Mining*, 395–405.
- Speith, T. 2022. A review of taxonomies of explainable artificial intelligence (XAI) methods. In *Proceedings of the 2022 ACM conference on fairness, accountability, and transparency*, 2239–2250.
- Spreitzer, N.; Haned, H.; and van der Linden, I. 2022. Evaluating the Practicality of Counterfactual Explanations. In *XAI. it@ AI* IA*, 31–50.
- Springenberg, J. T.; Dosovitskiy, A.; Brox, T.; and Riedmiller, M. 2014. Striving for simplicity: The all convolutional net. *arXiv preprint arXiv:1412.6806*.
- Srinivas, S.; and Fleuret, F. 2019. Full-gradient representation for neural network visualization. *Advances in Neural Information Processing Systems*, 32.
- Sun, Q.; Fang, Y.; Wu, L.; Wang, X.; and Cao, Y. 2023. Evalclip: Improved training techniques for clip at scale. *arXiv preprint arXiv:2303.15389*.
- Surden, H. 2021. Machine learning and law: An overview. *Research Handbook on Big Data Law*, 171–184.
- Taghipour, K.; and Ng, H. T. 2016. A neural approach to automated essay scoring. In *Proceedings of the 2016 Conference on Empirical Methods in Natural Language Processing*, 1882–1891.
- Vereschak, O.; Alizadeh, F.; Bailly, G.; and Caramiaux, B. 2024. Trust in AI-assisted Decision Making: Perspectives from Those Behind the System and Those for Whom the Decision is Made. In *Proceedings of the CHI Conference on Human Factors in Computing Systems*, 1–14.
- Wang, H.; Wang, Z.; Du, M.; Yang, F.; Zhang, Z.; Ding, S.; Mardziel, P.; and Hu, X. 2020. Score-CAM: Score-weighted visual explanations for convolutional neural networks. In *Proceedings of the IEEE/CVF Conference on Computer Vision and Pattern Recognition Workshops*, 24–25.
- Wang, Y.; Wang, C.; Li, R.; and Lin, H. 2022. On the use of BERT for automated essay scoring: Joint learning of multi-scale essay representation. *arXiv preprint arXiv:2205.03835*.
- Xiao, C.; Ma, W.; Xu, S. X.; Zhang, K.; Wang, Y.; and Fu, Q. 2024. From Automation to Augmentation: Large Language Models Elevating Essay Scoring Landscape. *arXiv preprint arXiv:2401.06431*.
- Xuan, Y.; Small, E.; Sokol, K.; Hettiachchi, D.; and Sander-son, M. 2023. Can Users Correctly Interpret Machine Learning Explanations and Simultaneously Identify Their Limitations? *arXiv preprint arXiv:2309.08438*.
- Xuan, Y.; Small, E.; Sokol, K.; Hettiachchi, D.; and Sander-son, M. 2025. Comprehension is a double-edged sword: Over-interpreting unspecified information in intelligible machine learning explanations. *International Journal of Human-Computer Studies*, 193: 103376.
- Yan, A.; Wang, Y.; Zhong, Y.; Dong, C.; He, Z.; Lu, Y.; Wang, W. Y.; Shang, J.; and McAuley, J. 2023. Learning concise and descriptive attributes for visual recognition. In *Proceedings of the IEEE/CVF International Conference on Computer Vision*, 3090–3100.
- Yang, R.; Cao, J.; Wen, Z.; Wu, Y.; and He, X. 2020. Enhancing automated essay scoring performance via fine-tuning pre-trained language models with combination of regression and ranking. In *Findings of the Association for Computational Linguistics: EMNLP 2020*, 1560–1569.
- Yang, S. C.-H.; Folke, N. E. T.; and Shafto, P. 2022. A psychological theory of explainability. In *International Conference on Machine Learning*, 25007–25021. PMLR.
- Yang, Y.; Zheng, Y.; Deng, D.; Zhang, J.; Huang, Y.; Yang, Y.; Hsiao, J. H.; and Cao, C. C. 2022. Hsi: Human saliency imitator for benchmarking saliency-based model explanations. In *Proceedings of the AAAI Conference on Human Computation and Crowdsourcing*, volume 10, 231–242.
- Yannakoudakis, H.; Briscoe, T.; and Medlock, B. 2011. A new dataset and method for automatically grading ESOL texts. In *Proceedings of the 49th Annual Meeting of the Association for Computational Linguistics: Human Language Technologies*, 180–189.
- Yeh, C.-K.; Hsieh, C.-Y.; Suggala, A.; Inouye, D. I.; and Ravikumar, P. K. 2019. On the (in) fidelity and sensitivity of explanations. *Advances in Neural Information Processing Systems*, 32.
- Zhai, X.; Mustafa, B.; Kolesnikov, A.; and Beyer, L. 2023. Sigmoid loss for language image pre-training. In *Proceed-*

ings of the IEEE/CVF international conference on computer vision, 11975–11986.

Zhang, R.; Isola, P.; Efros, A. A.; Shechtman, E.; and Wang, O. 2018. The unreasonable effectiveness of deep features as a perceptual metric. In *Proceedings of the IEEE conference on computer vision and pattern recognition*, 586–595.

A. PASTA-dataset: process

A.1 Generation of explanations

Classifier training The PASTA-dataset is designed to provide a benchmark for evaluating a wide range of XAI techniques across different explanation modalities. To ensure robustness and versatility, our dataset is based on four, publicly available datasets, each bringing distinct characteristics in terms of visual content and concept annotations. Choosing which task to focus on is a tough question. We have chosen to focus on image classification. This task can be performed in many different domains, but in order not to be too domain-specific, we decided to work on general datasets. These datasets enable the evaluation of both image-based and concept-based XAI methods.

Then, the initial phase in constructing the PASTA-dataset involves training the various classifier models on which explanations will be generated. Specifically, we utilize ResNet50 (He et al. 2016), ViT-B (Dosovitskiy 2020), ResNet50-BCos (Böhle et al. 2024), CLIP-Linear (Yan et al. 2023), CLIP-QDA (Kazmierczak et al. 2024), X-NeSyL (Díaz-Rodríguez et al. 2022), and CBM (Koh et al. 2020). These models are trained separately on each classifier’s dataset referenced below.

It is important to note that certain classifiers utilized in our platform necessitate concept-level annotations. Specifically, for each sample, information regarding the presence or absence of each concept in the image, along with their respective bounding boxes, is required. This detailed information is not natively available in each dataset. Consequently, we enhanced each dataset to meet this requirement. The datasets and the corresponding modifications are as follows:

- **COCO:** A widely-used dataset known for its complexity and variety, containing 117k training images, 4.5k validation images annotated with 80 object categories, which we consider to be concepts in the images. The labels correspond for this specific dataset to indoor scene labeling, to do so, we took the subset of images of indoor scenes (53,051 images). Then, we labeled the images using a scene label DNN trained on the MIT SUN.
- **Pascal Part:** This dataset focuses on detailed part-level annotations, providing fine-grained insights into object structure and component relationships. It is composed of 13,192 training images, 39 concepts, and 16 classes.
- **Cats Dogs Cars:** A curated dataset featuring images of cats, dogs, and cars. The goal of this dataset is to explore if color biases are present in the model or not. It is composed of 3,858 training images, 39 concepts, and 3 classes. Since this network does not include annotated concepts, we used Grounding DINO (Liu et al. 2023) as an annotator. Since the number of images that constitute Cate Dogs Cars is sufficiently small, we manually checked the bounding boxes generated and found no significant errors.
- **Monumai:** A specialized dataset containing images of monuments, with annotations that include both the overall structures and specific architectural features. It is composed of 908 images, 15 concepts, and 4 classes.

Each dataset in the classifier’s training datasets is annotated at two levels:

- **Image-level annotations:** These are traditional class labels (Table 4) or object categories that describe the primary content of the image.
- **Concept-level annotations:** These describe specific, human-understandable features within the image, enabling the application of Concept Bottleneck Models (CBMs) and other concept-based XAI methods. The list of concepts for each dataset is detailed in Table 3.

Table 3: **List of concepts used in all our CBMs.** For each *Dataset* used, we choose a different set to fit the annotations.

<i>Dataset</i>	<i>Concepts</i>
catsdogscars, pascalpart	engine, artifact_wing, animal_wing, stern, tail, locomotive, arm, hair, wheel, chain_wheel, handlebar, hand, headlight, saddle, body, bodywork, beak, head, eye, foot, leg, neck, torso, cap, license_plate, door, mirror, window, ear, muzzle, horn, nose, hoof, mouth, eyebrow, plant, pot, coach, screen
monumai	horseshoe-arch, lobed-arch, pointed-arch, ogee-arch, trefoil-arch, serliana, solomonic-column, pinnacle-gothic, porthole, broken-pediment, rounded-arch, flat-arch, segmental-pediment, triangular-pediment, lintelled-doorway
coco	person, backpack, umbrella, handbag, tie, suitcase, bicycle, car, motorcycle, air-plane, bus, train, truck, boat, traffic light, fire hydrant, stop sign, parking meter, bench, bird, cat, dog, horse, sheep, cow, elephant, bear, zebra, giraffe, frisbee, skis, snowboard, sports ball, kite, baseball bat, baseball glove, skateboard, surfboard, tennis racket, bottle, wine glass, cup, fork, knife, spoon, bowl, banana, apple, sandwich, orange, broccoli, carrot, hot dog, pizza, donut, cake, chair, couch, potted plant, bed, dining table, toilet, tv, laptop, mouse, remote, keyboard, cell phone, microwave, oven, toaster, sink, refrigerator, book, clock, vase, scissors, teddy bear, hair drier, toothbrush

Table 4: List of classes used in all the datasets used to train our inference models.

<i>Dataset</i>	<i>Labels</i>
catsdogscars	cat, dog, car
pascalpart	aeroplane, bicycle, bird, bottle, bus, car, cat, cow, dog, horse, motorbike, person, pottedplant, sheep, train, tvmonitor
monumai	Baroque, Gothic, Hispanic-Muslim, Renaissance
coco	shopping_and_dining, workplace, home_or_hotel, transportation, sports_and_leisure, cultural

In Figure 10, we observe the class distribution across the different datasets. While the distributions are not perfectly uniform, they generally reflect the original composition of the datasets, ensuring that the diversity of the data is preserved in the evaluation process.

As previously indicated, additional care must be taken when training CBMs. To explain the various training procedures for our CBMs, we decompose them into two components: the concept extractor and the classifier. The concept extractor generates an embedding from an input image, with each element representing a concept, while the classifier predicts the label from this embedding. We categorize the CBMs we use based on the training methods for these two components. For CLIP-based CBMs (LaBo, CLIP-linear, and CLIP-QDA), the concept extraction is performed in a zero-shot manner *i.e.*, we only use the training images and labels to train the classifier. For CBMs that require training the concept extractor (X-NeSyL and ConceptBottleneck), we use the concept annotations provided by each dataset.

For explanations that involve the application of post-hoc techniques on black-box models, we selected the following DNNs: ResNet 50, ViT, and CLIP (zero-shot). For ResNet 50 and ViT, a separate network was trained for each dataset. For CLIP (zero-shot), we followed the standard procedure proposed by Radford et al. (2021), which classifies by selecting the highest similarity score between the image embedding and all the text embeddings. For post-hoc explanations, we directly extract the explanation after training.

As illustrated in Figure 11, the models used in this study achieve an accuracy of at least 59%. Notably, one of the models, the zero-shot CLIP, exhibits difficulty specifically with the Monumai dataset, which explains some of the performance variability. Despite this, the overall accuracy of the models remains relatively consistent across datasets. For CBMs, achieving high accuracy across all models required certain compromises, particularly with respect to the concepts used. Although for uniformity we used the same concept sets across different models, it was not always guaranteed that the trained model is the best model.

Computation of explanations Upon completion of the training process for all classifiers, the subsequent phase involves the generation of explanations for their respective inferences. A comprehensive enumeration of the XAI methods, along with the corresponding classifiers to which each method is applied, is presented in Table 5. For this, we use for the computation of explanations a subset of 250 images of the classifier’s dataset test split per dataset, that serve as the basis of the PASTA-dataset. This diverse selection ensures a broader generalization of the XAI techniques across datasets being assessed. Note that, unlike traditional datasets, our benchmark dataset comprises a triplet of images, explanations, and labels. This triplet enables us to quantitatively assess the quality of XAI techniques.

Precisely, we tested 14 saliency-based XAI techniques and 6 concept-based XAI techniques, with a particular emphasis on a variety of functioning of methods. A beneficial aspect of our approach is that many of the methods are tested on multiple backbone architectures. This aspect is particularly important, as many of the post-hoc methods evaluated in our study are designed to be DNN-agnostic. In such cases, the XAI method is applied to independently trained models. For instance, GradCAM is evaluated on ResNet50, ViT-B, and CLIP-zero-shot models, while SHAP-CBM is applied to both CLIP-QDA and the original Concept Bottleneck model as proposed by Koh et al. (2020).

A brief description of each method is provided below to summarize their key features and mechanisms.

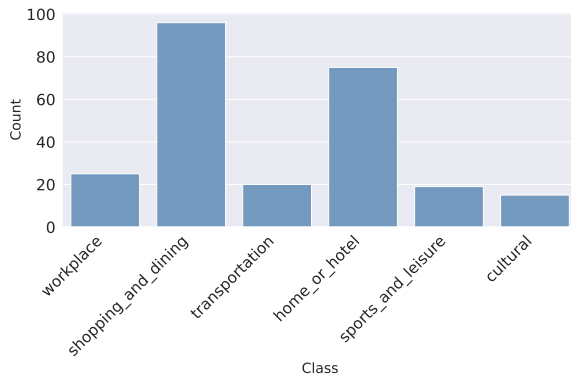
LIME (Local Interpretable Model-agnostic Explanations): LIME explains individual predictions of any classifier by approximating it locally with an interpretable model. It perturbs the input and observes how the predictions change, identifying the most influential parts of the input for the prediction.

SHAP (SHapley Additive exPlanations): SHAP is a unified approach to interpreting model predictions based on Shapley values from cooperative game theory. It assigns each feature an importance value for a particular prediction, offering a sound measure of feature importance.

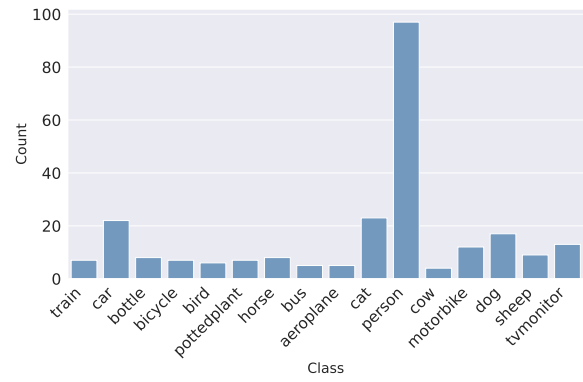
GradCAM (Gradient-weighted Class Activation Mapping): GradCAM visualizes the regions in an image that contribute to the classification. It uses the gradients of the target concept (e.g., a specific class) flowing into the final convolutional layer to produce a coarse localization map highlighting important regions.

AblationCAM: AblationCAM improves GradCAM by iteratively removing parts of the input and observing the output effect to identify important regions.

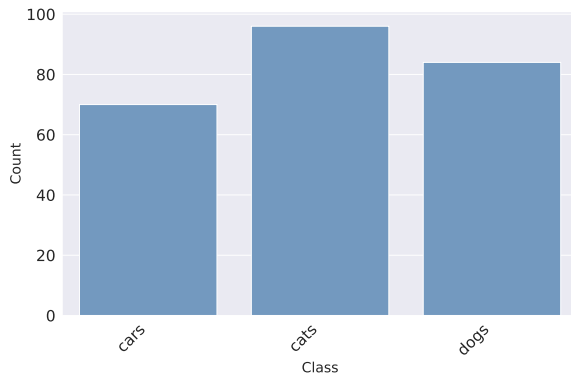
EigenCAM: EigenCAM applies PCA to the activations of the last convolutional layer to produce a saliency map. It highlights



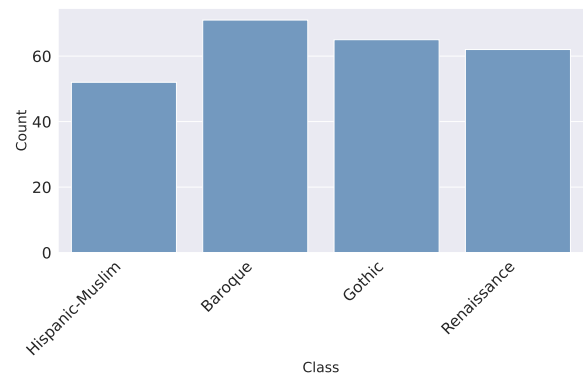
COCO



Pascal Part



Cats Dogs Cars



Monumai

Figure 10: **Class distribution across the different test sets.**

the directions in which activations show the most variance, identifying critical features.

FullGrad: FullGrad computes gradients of the output with respect to both the input and intermediate layer outputs, aggregating these gradients to generate a comprehensive saliency map.

GradCAMPlusPlus: GradCAMPlusPlus improves GradCAM with a refined weighting scheme for the gradients, allowing better handling of multiple occurrences of the target concept.

GradCAMElementWise: GradCAMElementWise extends GradCAM by considering element-wise multiplications of gradients and activations, producing more precise visual explanations.

HiResCAM: HiResCAM improves on class activation mapping by using higher-resolution feature maps for more detailed visual explanations.

ScoreCAM: ScoreCAM improves CAM methods by using output scores to weight the activation maps' importance, providing a more faithful saliency map without relying on gradients.

XGradCAM: XGradCAM integrates cross-layer information to combine saliency maps from different layers.

DeepFeatureFactorization: This method decomposes feature representations learned by a deep model into interpretable factors. It provides insights into how features contribute to the model's decisions.

CLIP-QDA-sample: This model uses the CLIP framework and applies Quadratic Discriminant Analysis (QDA) for classification. This methodology employs counterfactuals on the conceptual representations of images to generate explanations.

CLIP-Linear-sample: This model also uses the CLIP framework but employs logistic regression for classification, thereby offering interpretable explanations grounded in the transparency of the regression analysis.

X-NeSyL: X-NeSyL identifies concepts using object detection and applies a small DNN to these concepts, using the weights assigned to each concept for explanation.

LIME CBM: This model generates a list of concepts and applies logistic regression. The methodology employs LIME to identify and highlight the most significant concepts at the conceptual level for classification purposes.

SHAP CBM: This model generates a list of concepts and applies logistic regression, using SHAP on the concept level to emphasize the most crucial concepts in classification.

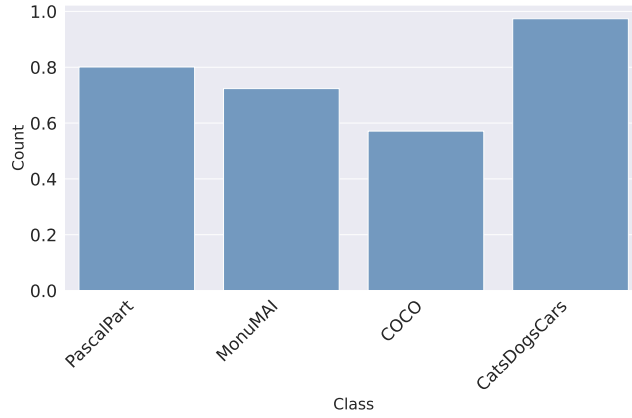


Figure 11: Accuracy across the different test sets of the different models.

Labo: Similar to CLIP-Linear-sample, Labo extracts human-interpretable concepts and maps them to the model’s internal representations to facilitate more comprehensible decision-making explanations. This process leverages the transparency of its classification mechanism, albeit utilizing a custom transparent network.

RISE: RISE (Randomized Input Sampling for Explanation) generates heatmaps by perturbing input regions and measuring their impact on model outputs. This technique identifies the most influential regions in the model’s decision-making process.

BCos: BCos introduces specific layers to encourage alignment between weights and activation maps, which can then be used for explainability.

The PASTA dataset comprises 21,100 instances, each containing images, predictions, and explanations. These instances were subsequently evaluated by human annotators, resulting in 633,000 unique Likert ratings. This extensive evaluation was achieved by asking six questions to five annotators for each instance. We aggregate these evaluations using majority voting to favor consensus opinions. This dataset size is fairly standard in the Automated Essay Scoring literature (Lee et al. 2024), where the objective is to train a model to predict human-assigned scores. Figure 12 shows the distribution of XAI techniques applied across the datasets. To enhance the generalizability of our results, we increased the diversity of XAI techniques used. This was achieved by not applying every technique to every image uniformly, allowing for a more diverse set of explanations to be generated. This variability ensures that our analysis captures a broad spectrum of interpretability techniques, providing deeper insights into the performance of XAI techniques across different datasets and models.

A.2 Human evaluation protocol

Once the explanations are performed, we can quantify the interpretability and usefulness of XAI techniques accurately, using a human evaluation of the quality of explanations. Our human-centric approach complements existing approaches that focus primarily on assessing the model’s internal behavior. For example, traditional evaluations of *faithfulness* measure how closely an explanation corresponds to the model’s true functioning, while we assess in our dataset how the explanation fits human expectations.

Desiratas First, we establish a comprehensive set of assessment criteria that are evaluated on a graded scale. We consolidate different criteria from the literature into the following set of *desiderata* for XAI explanations that we wish to evaluate:

- *Trustworthiness* (Arrieta et al. 2020) measures the extent to which an explanation accurately reflects whether a model will act as intended when facing a given problem.
- *Robustness* (Doshi-Velez and Kim 2017; Agarwal et al. 2022a; Yeh et al. 2019) assesses the stability and relevance of the explanation across a broad range of models and inputs.
- *Complexity* (Nauta et al. 2023; Nguyen and Martínez 2020; Bhatt, Weller, and Moura 2021) checks whether the explanation is both simple and informative, balancing clarity and detail.
- *Objectivity* (Bennetot et al. 2022) evaluates whether the explanation is interpreted consistently by the majority within a given audience.

Evaluation Protocol Then, we apply an evaluation protocol, developed with the help of a psychologist, to ensure that annotators fully understand the task and the expectations. This includes annotator training and close monitoring throughout the process. Interfaces, as well as the formulation of questions, play a key role in the quality of the annotations (Pommeranz et al. 2012), and their design must be considered cautiously to avoid confounding cognitive biases. The formulation of the questions

Table 5: **XAI methods included in our dataset.** *Name* denotes the identifier of the utilized XAI method. *Functioning* specifies the mechanism of the explanation computation, including methods that rely on gradient weighting (Gradient), probing reactions to localized perturbations (Perturbation), abstracting activations through factorization (Factorization), leveraging directly interpretable latent spaces (Interpretable latent space), or searching for counterfactuals (Counterfactual). *Attribution* indicates the data type on which the attribution weights are applied: either on input images (Image) or on a computed representation of the image as concepts (Concepts). *Stage* indicates whether the explanation is produced by an ante-hoc or a post-hoc process.

<i>Name</i>	<i>Functioning</i>	<i>Attribution on</i>	<i>Stage</i>	<i>Applied on</i>
BCos (Böhle et al. 2024)	Interpretable latent space	Image	Ante-hoc	ResNet50-BCos
GradCAM (Selvaraju et al. 2017)	Gradient	Image	Post-hoc	ViT, ResNet50, CLIP (zero-shot)
HiResCAM (Draelos and Carin 2020)	Gradient	Image	Post-hoc	ViT, ResNet50, CLIP (zero-shot)
GradCAMElementWise (Pillai and Pirsiavash 2021)	Gradient	Image	Post-hoc	ViT, ResNet50, CLIP (zero-shot)
GradCAM++ (Chattopadhyay et al. 2018)	Gradient	Image	Post-hoc	ViT, ResNet50, CLIP (zero-shot)
XGradCAM (Fu et al. 2020)	Gradient	Image	Post-hoc	ViT, ResNet50, CLIP (zero-shot)
AblationCAM (Ramaswamy et al. 2020)	Perturbation	Image	Post-hoc	ViT, ResNet50, CLIP (zero-shot)
ScoreCAM (Wang et al. 2020)	Perturbation	Image	Post-hoc	ViT, ResNet50
EigenCAM (Muhammad and Yeasin 2020)	Factorization	Image	Post-hoc	ViT, ResNet50, CLIP (zero-shot)
EigenGradCAM (Muhammad and Yeasin 2020)	Gradient+Factorization	Image	Post-hoc	ViT, ResNet50, CLIP (zero-shot)
FullGrad (Srinivas and Fleuret 2019)	Gradient	Image	Post-hoc	ViT, ResNet50
Deep Feature Factorizations (Collins, Achanta, and Susstrunk 2018)	Factorization	Image	Post-hoc	ViT, ResNet50, CLIP (zero-shot)
SHAP (Lundberg and Lee 2017)	Perturbation	Image	Post-hoc	ViT, ResNet50, CLIP (zero-shot)
LIME (Ribeiro, Singh, and Guestrin 2016)	Perturbation	Image	Post-hoc	ViT, ResNet50, CLIP (zero-shot)
X-NeSyL (Díaz-Rodríguez et al. 2022)	Interpretable latent space	Concepts	Ante-hoc	X-NeSyL
CLIP-linear-sample (Yan et al. 2023)	Interpretable latent space	Concepts	Ante-hoc	CLIP-linear
CLIP-QDA-sample (Kazmierczak et al. 2024)	Counterfactual	Concepts	Ante-hoc	CLIP-QDA
LIME-CBM (Kazmierczak et al. 2024)	Perturbation	Concepts	Post-hoc	CLIP-QDA, ConceptBottleneck
SHAP-CBM (Kazmierczak et al. 2024)	Perturbation	Concepts	Post-hoc	CLIP-QDA, ConceptBottleneck
RISE-CBM (Petsiuk, Das, and Saenko 2018)	Perturbation	Concepts	Post-hoc	ConceptBottleneck

has been carefully chosen to ensure that they are fully understood by each annotator. To maintain consistency and reliability, all annotators undergo a training session before starting the actual annotation task. This training familiarizes them with the XAI techniques, evaluation criteria, rating scale and datasets, ensuring a uniform understanding of the task and the expectations.

The annotation process took place via an online web application, created and deployed by a contracting company. 24 participants were recruited to take part in the annotation process. These participants ranged in age from 19 to 37 (mean age 24.58, standard deviation 3.19). Figure 13 shows the age distribution. Among the participants, 7 identified themselves as male, 17 as female, 0 as non-binary, 0 did not wish to say. All participants were based in India. Each participant’s task was to annotate 147 explanations. To address the subjectivity inherent in the task, each instance, comprising a triplet of image, explanation, and label, is evaluated by five different annotators.

Concretely, annotators are shown a succession of samples that consist in an image, a prediction, and an explanation. They are then asked to respond to a set of questions corresponding to the desiderata outlined above (indicated in *italics*):

- Q1: Is the provided explanation consistent with how I would explain the predicted class? *Trustworthiness*
- Q2: Overall the explanation provided for the model prediction can be trusted? *Trustworthiness*
- Q3: Is the explanation easy to understand? *Complexity*
- Q4: Can the explanation be understood by a large number of people, independently of their demographics (age, gender, country, etc.) and culture? *Objectivity*
- Q5: With this perturbed image, to what extent has the explanation changed ? (Examples with good predictions and light perturbations) *Robustness*
- Q6: With this perturbed image, to what extent has the explanation changed? (Examples with bad predictions and strong perturbations) *Robustness*

A screenshot of the interface used by the annotators to answer is available in Figure 14. The first four questions (Q1 to Q4) concerned Section 1, which showed the original image on the left and the explanation on the right. These first four questions enabled participants to assess the levels of reliability, complexity and objectivity of the explanation. The fifth question (Q5) concerned Section 2, showing the slightly disturbed original image and the corresponding explanation. The sixth question (Q6) concerned Section 3, showing a more disturbed image and the corresponding explanation. These last two questions were intended to assess the robustness of the XAI technique. For each question, participants had to answer with a 5-point Likert scale. In question 5, we apply a weak data augmentation to the input image, which is designed to preserve the classifier’s prediction. This allows us to evaluate whether the explanation changes when the prediction remains constant. Measuring changes in explanations is challenging, as studied by (Fel et al. 2022b). To address this, we leverage human evaluators who can more effectively discern subtle changes in explanations. Q6 follow a similar approach but involve strong data augmentation. The goal here is to determine if the explanations remain consistent when the predictions change due to data augmentation or variations in the

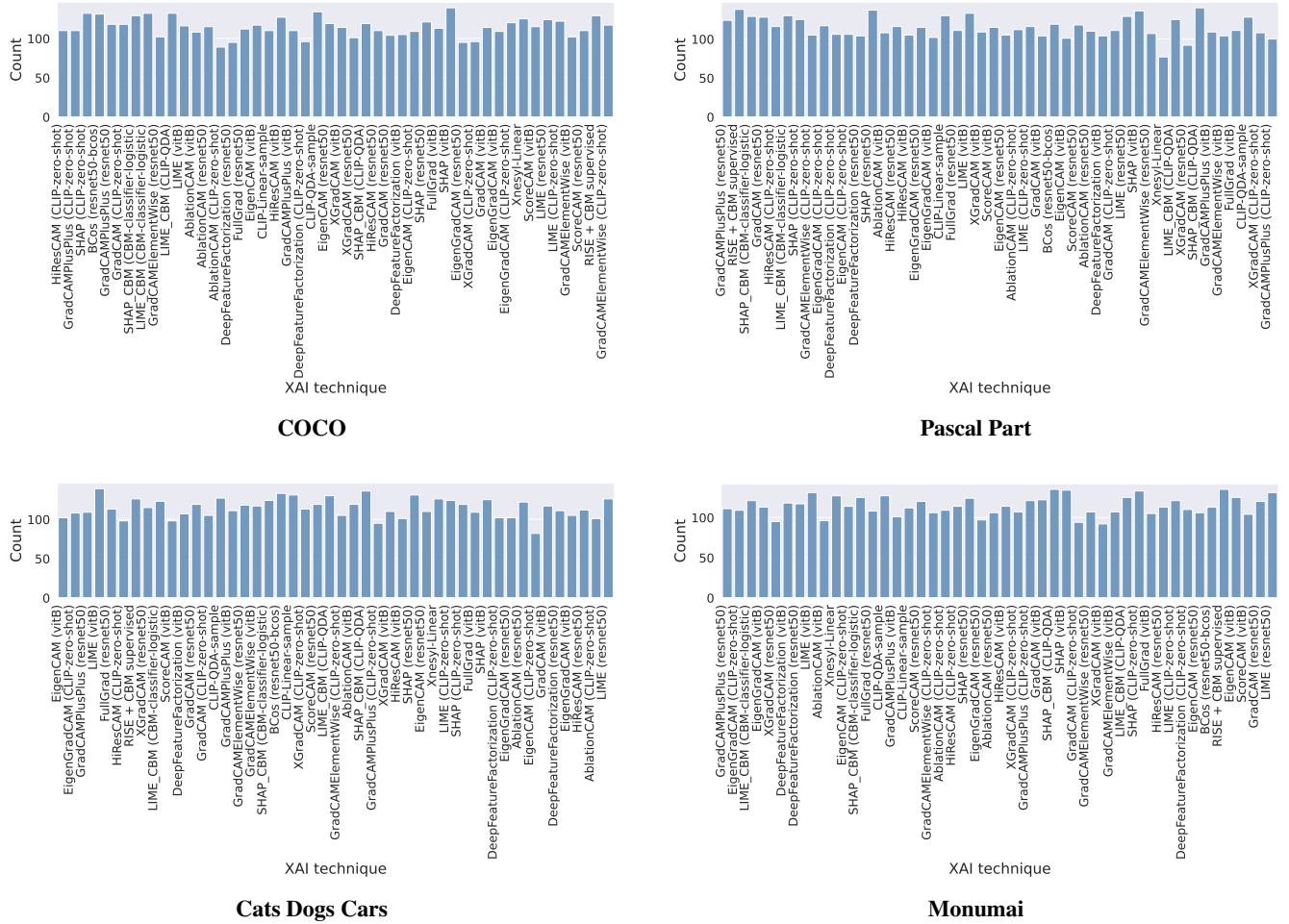


Figure 12: Distribution across the different XAI techniques across the different datasets.

models. If the predictions change, the explanations should reflect these changes. For more details, refer to Figure 15.

We outline the perturbation process below. To capture a diverse range of model responses, we applied 12 distinct types of perturbations, each with a tunable magnitude parameter to adjust perturbation intensity. The transformations include both standard torchvision operations (<https://pytorch.org/vision/0.9/transforms.html>) and custom-designed modifications:

- **Color Jitter (Brightness):** Adjusts the brightness of the image. The magnitude lower the brightness.
- **Color Jitter (Contrast):** Modifies image contrast. The magnitude lower the contrast.
- **Random Resized Crop:** Performs a random crop and resize. The magnitude augments the scale of the crop.
- **Gaussian Blur:** Blurs the image using a Gaussian filter. The magnitude augments the values of the standard deviation.
- **Random Perspective:** Applies a perspective transformation. The magnitude augments the distortion scale.
- **Brightness Transform:** Independently changes brightness levels. The magnitude lower the brightness.
- **Color Transform:** Adjusts color balance. The magnitude augments the saturation.
- **Contrast Transform:** Further modifies contrast. The magnitude augments the contrast.
- **Sharpness Transform:** Changes image sharpness. The magnitude augments the sharpness factor.
- **Posterize Transform:** Reduces color depth. The magnitude augments the number of bits to keep for each channel.
- **Solarize Transform:** Inverts colors above a certain threshold. The magnitude augments the threshold.
- **Random Masking:** Masks out random sections of the image by applying patches. The magnitude augments the number of patches.

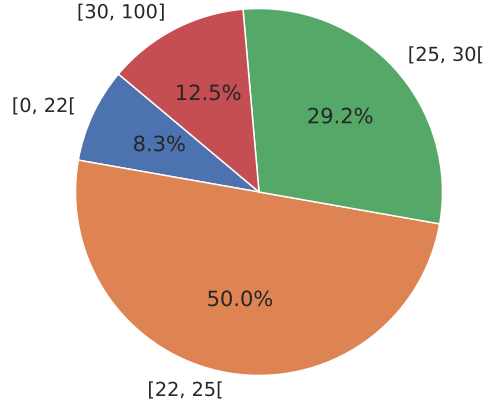


Figure 13: **Age distribution of the annotators.**

Our aim was to avoid influencing responses and to eliminate any ambiguities that could lead to inaccurate answers. Human decision-making, especially when it involves assessing the quality of explanations, is complex. To address this, we provided training on deep learning and various XAI techniques, ensuring the content was clearly understandable by the annotators. After the initial training, the annotators answered the questions, and we held weekly meetings to clarify any confusion they encountered.

Each explanation is rated on a five points Likert scale, where one star indicates a total disagreement with the annotator’s reasoning, and five stars represent total agreement.

B. PASTA-dataset: Additional analysis

B.1 Comparison with existing benchmark

We compiled a set of related works that perform human assessment in the context of XAI. Specifically, we noted key details such as the dataset size, the number of participants involved, the diversity of questions posed, and the overall scope of the study, where this information was available. A summary of these details is presented in Table 6.

The PASTA-dataset distinguishes itself in several key aspects. First, it evaluates a significantly higher number of XAI methods compared to existing datasets. This design emphasizes the diversity of techniques over the number of samples tested, offering a complementary approach to datasets that prioritize varied input data but evaluate fewer methods. Second, PASTA involves the lowest number of participants among the datasets listed, allowing for reduced variability due to potential outliers and better control over annotator behavior. However, this could introduce inherent biases tied to the limited participant pool. Finally, the PASTA-dataset provides a substantially larger number of samples and uniquely combines image-based explanations with concept-based explanations, making it the first dataset to address both modalities simultaneously.

B.2 Comparison with existing metrics

Faithfulness: *How much does the explanation describe the true behavior of the model?* A number of different ways to compute *faithfulness* exist, but they all broadly fit the same framework of measuring how much model predictions change in response to input perturbations (Bhatt, Weller, and Moura 2021; Alvarez-Melis and Jaakkola 2018a; Yeh et al. 2019; Rieger and Hansen 2020; Arya et al. 2019; Nguyen and Martínez 2020; Bach et al. 2015; Samek et al. 2016; Montavon, Samek, and Müller 2018; Ancona et al. 2017; Dasgupta, Frost, and Moshkovitz 2022). Intuitively, an explanation is faithful if perturbing regions deemed irrelevant by the explanation bring little to no change in model output, whereas perturbing regions deemed relevant bring a considerable change. In this analysis, we resort to the evaluation protocol outlined in Azzolin et al. (2025), which generalized a number of common *faithfulness* metrics into a common mold¹. Specifically, *faithfulness* is estimated as the harmonic mean of **sufficiency** (Suf) and **necessity** (Nec), which account for the degree of prediction changes after perturbing irrelevant or relevant portions of the input, respectively. Formally, given an input image x with associated explanation e , and a

¹They focus on *faithfulness* for graph explanations, but the evaluation protocol is aligned with that of images.



Figure 14: **Screenshot of the annotation interface.** Questions are on the right-part of the interface. Middle panel shows Section 2: slightly disturbed original image with the explanation.





model to be explained $p_\theta(Y \mid \mathbf{x})$, sufficiency and necessity are defined as:

$$\begin{aligned} \text{Suf}_{d,p_R}(\mathbf{x}, \mathbf{e}) &= \mathbb{E}_{\mathbf{x}' \sim p_R} [d(p_\theta(\cdot \mid \mathbf{x}) \parallel p_\theta(\cdot \mid \mathbf{x}'))] \\ \text{Nec}_{d,p_C}(\mathbf{x}, \mathbf{e}) &= \mathbb{E}_{\mathbf{x}' \sim p_C} [d(p_\theta(\cdot \mid \mathbf{x}) \parallel p_\theta(\cdot \mid \mathbf{x}'))], \end{aligned} \quad (5)$$

where d is a divergence between distributions of choice, and p_C and p_R are interventional distributions specifying the set of allowed perturbations to the explanation and its complement, respectively. Eq. 5 are then normalised to $[0, 1]$, the higher the better, via a non-linear transformation, i.e., taking $\exp(-\text{Suf}_{d,p_R}(\mathbf{x}, \mathbf{e}))$ and $1 - \exp(-\text{Nec}_{d,p_C}(\mathbf{x}, \mathbf{e}))$. Operationally, for a given instance (\mathbf{x}, \mathbf{e}) sampling from $p_C(\mathbf{x}, \mathbf{e})$ equals to generating a new image where the complement of the explanation is left intact, and where perturbations are applied to the explanation. The set of allowed perturbations p_C and p_R can be arbitrarily defined, and different techniques are oftentimes reported to give different interpretations (Hase, Xie, and Bansal 2024; Rong et al. 2022). To avoid this confounding effect, we report the results for three different baseline perturbations, namely uniform and Gaussian noise, and black patches, along with a more advanced information-theoretic strategy named ROAD (Rong et al. 2022). Since explanations are oftentimes in the form of soft relevance scores over the entire input, a threshold is needed to tell apart relevant from irrelevant image regions. To avoid relying upon this hard-to-define hyperparameter, we aggregate the scores across multiple thresholds keeping only the best value. Therefore, for each explanation threshold value, pixels are sorted based on their relevance² and progressively perturbed until reaching the fixed threshold value, while leaving the others unchanged. For each of those samples, we evaluate the normalized Eq. 5 where d is the absolute difference in class-predicted confidence between clean and perturbed images, i.e., $|p_\theta(\hat{y} \mid \mathbf{x}) - p_\theta(\hat{y} \mid \mathbf{x}')|$, and average across the number of perturbed pixel for each threshold value. This procedure is detailed in Algorithm 1. Considering the novelty of our human driven study and the existence of such metrics, an interesting experiment is to measure if the the rating given by humans correlate with ROAD. Results, shown in Table 7 indicates a rather weak correlation. We conclude that our human scores indeed cover an aspect of explanation quality unrelated to that of perceptual quality, as predicted by Biessmann and Refiano (2021). The results cover only




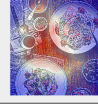
²For sufficiency, pixels are sorted in ascending order. For necessity, in descending order.

Q5: With this perturbed image, to what extent has the explanation changed ?

	Original image	Perturbed image
Input image		
Prediction of the model	'shopping and dining'	'shopping and dining'
Explanation of the model's decision		

(a) A light perturbation is applied, resulting in no label change.

Q6: With this perturbed image, to what extent has the explanation changed ?

	Original image	Perturbed image
Input image		
Prediction of the model	'shopping and dining'	'cultural'
Explanation of the model's decision		

(b) A strong perturbation is applied, leading to a label change.

Figure 15: Samples corresponding to questions 5 and 6.

Table 6: **Overview of datasets and human evaluation frameworks for XAI methods.** *Name* refers to the reference of the dataset used. *Annotations* refers to the type of labels used: Likert refers to Likert scale, Saliency refers to pseudo saliency maps, 2AFC refers to two alternative forced choices, Clicktionary refers to the clicktionary game defined in (Dawoud et al. 2023), MCQ refers to multiple-choice question, and Binary refers to binary choices. $N_{Samples}$ refers to the total number of samples constituting the dataset. N_{Part} refers to the number of participants involved during the labeling. *Modality* refers to the different modalities the dataset deals with: I refers to image, C to concepts, and T to text. N_Q refers to the number of different questions asked to the annotators. N_{XAI} refers to the number of XAI methods tested during the experiments, *No* indicates that the dataset only asked to label data with what they consider as ground truth explanation, without further comparison with XAI methods. N_{Data} refers to the number of different samples (for example images) shown to annotators.

Name	Annotations	$N_{Samples}$	N_{Part}	Modality	N_Q	N_{XAI}	N_{Data}
PASTA-dataset	Likert	633,000	24	I + C	6	20	1000
Yang, Folke, and Shafto (2022)	Saliency, 2AFC	356	46	I	2	1	89
Colin et al. (2022)	Classification	1,960	241	I	1	6	NA
Dawoud et al. (2023)	Clicktionary	3,836	76	I	1	3	102
Mohseni, Block, and Ragan (2021)	Saliency	1,500	200	I + T	1	<i>No</i>	1,500
Herm et al. (2021)	Likert	NA	165	C	1	6	NA
Morrison et al. (2023)	Clicktionary/QCM	450	50	I	1	3	39
Spreitzer, Haned, and van der Linden (2022)	Likert/Binary	4,050	135	C	9	2	NA
Xuan et al. (2023)	Likert/Binary	3,600	200	C	4	2	1,326

image-level attribution methods (see Table 5), as CBMs do not support such kinds of input-level manipulations. Our findings reinforce the idea that human evaluations and computational metrics measure complementary aspects of XAI methods. Human evaluations excel at assessing the usefulness of explanations, aligning with their primary purpose of serving a human audience. In contrast, computational metrics, such as faithfulness, focus on evaluating the alignment between the explanation and the model’s actual internal functioning. This aspect lies beyond the reach of human judgment, as humans cannot directly access or fully comprehend the internal mechanisms of the model. Evaluating the quality of an explanation typically involves estimating different and potentially orthogonal aspects of it. In addition to the perceptual quality addressed in this work, others can be numerically simulated by having access to model weights. In this additional analysis, we consider some of those aspects and measure how much they correlate with human scores.

Robustness: *Robustness* roughly refers to how stable the explanation is to small input perturbations. Different ways to estimate it exist (Alvarez-Melis and Jaakkola 2018b; Montavon, Samek, and Müller 2018; Yeh et al. 2019; Dasgupta, Frost, and Moshkovitz 2022; Agarwal et al. 2022a). In our analysis, we focused on MaxSensitivity (Yeh et al. 2019), which applies random input perturbations to the entire image and measures the pixel-wise difference between the original explanation, and the one obtained on the perturbed sample. Formally:

$$\text{MaxSensitivity} = \max \|e - e'\| \quad (6)$$

where e and e' are the explanations for the original and the perturbed image, respectively. Again, different perturbation techniques can be applied, and we resort to the two simple baselines, namely Uniform and Gaussian noise. No normalization is

Table 7: **Pearson Correlation Coefficient (PCC) and Spearman rank Correlation Coefficient (SCC) between *faithfulness* computed with different methods and human scores.** Values are presented with p-values in parentheses.

	ROAD		Black patches		Uniform noise		Gaussian noise	
	PCC	SCC	PCC	SCC	PCC	SCC	PCC	SCC
Q1	0.029 (1e-4)	-0.047 (8e-10)	0.111 (1e-47)	0.077 (1e-23)	0.037 (1e-6)	-0.036 (2e-6)	0.036 (1e-6)	-0.032 (3e-5)
Q2	0.030 (1e-4)	-0.044 (1e-9)	0.108 (3e-45)	0.075 (2e-22)	0.034 (9e-6)	-0.037 (1e-6)	0.034 (1e-5)	-0.032 (3e-5)
Q3	0.035 (6e-6)	0.003 (7e-1)	0.079 (3e-25)	0.065 (2e-17)	0.029 (2e-4)	0.005 (5e-1)	0.027 (1e-4)	0.004 (6e-1)
Q4	0.033 (1e-5)	-0.008 (3e-1)	0.081 (3e-26)	0.062 (1e-15)	0.030 (9e-5)	-0.001 (9e-1)	0.029 (2e-4)	-0.001 (9e-1)
Q5	-0.060 (8e-15)	0.003 (7e-1)	-0.067 (3e-18)	-0.028 (1e-4)	-0.066 (6e-18)	-0.025 (1e-3)	-0.065 (3e-17)	-0.022 (4e-3)
Q6	-0.019 (1e-2)	0.059 (1e-14)	-0.053 (4e-12)	-0.031 (6e-5)	-0.023 (1e-3)	0.029 (1e-4)	-0.022 (5e-3)	0.030 (1e-4)

Algorithm 1: Pseudo code for computing sufficiency/necessity

Require: Image \mathbf{x} , explanation e , and set of explanation-size thresholds \mathcal{T} .

```

1: values = []
2: for each threshold  $t \in \mathcal{T}$  do
3:   if computing sufficiency then
4:     Sort pixels of  $\mathbf{x}$  in ascending order of relevance scores from  $e$ .
5:   else
6:     Sort pixels of  $\mathbf{x}$  in descending order of relevance scores from  $e$ .
7:   end if
8:   arr  $\leftarrow$  []
9:   for  $i$  in range(start=1, end= $t$ , step=2) do
10:     $\mathbf{x}' \leftarrow$  Apply the specified perturbations to the first  $i\%$  sorted pixels.
11:    Append  $d = |p_\theta(\hat{y} | \mathbf{x}) - p_\theta(\hat{y} | \mathbf{x}')|$  to arr
12:   end for
13:   if computing sufficiency then
14:     Append  $\exp(-\text{mean}(\text{arr}))$  to values
15:   else
16:     Append  $1 - \exp(-\text{mean}(\text{arr}))$  to values
17:   end if
18: end for
19: Output:  $\max(\text{arr})$ 

```

Table 8: **Pearson Correlation Coefficient (PCC) and Spearman rank Correlation Coefficient (SCC) between MaxSensitivity computed with different perturbation strategies and human scores.** In parentheses, the respective p-values.

	Uniform noise		Gaussian noise	
	PCC	SCC	PCC	SCC
Q1	-0.262 (9e-178)	-0.326 (4e-280)	-0.250 (4e-165)	-0.301 (7e-243)
Q2	-0.258 (4e-172)	-0.323 (4e-273)	-0.247 (2e-161)	-0.297 (7e-236)
Q3	-0.164 (7e-69)	-0.193 (3e-95)	-0.175 (1e-80)	-0.188 (3e-93)
Q4	-0.176 (6e-80)	-0.201 (2e-103)	-0.182 (8e-88)	-0.190 (3e-95)
Q5	0.136 (9e-48)	0.169 (1e-73)	0.104 (2e-29)	0.103 (6e-29)
Q6	0.101 (5e-27)	0.125 (5e-41)	0.100 (3e-27)	0.132 (1e-46)

Table 9: **Pearson Correlation Coefficient (PCC) and Spearman rank Correlation Coefficient (SCC) between Sparseness and human scores.** In parentheses the respective p-values.

	Complexity	
	PCC	SCC
Q1	-0.137 (4e-72)	-0.134 (3e-69)
Q2	-0.134 (6e-69)	-0.131 (5e-66)
Q3	-0.080 (3e-25)	-0.075 (9e-23)
Q4	-0.079 (6e-25)	-0.073 (2e-21)
Q5	-0.085 (1e-28)	-0.087 (6e-30)
Q6	0.052 (9e-12)	0.073 (9e-22)

applied, therefore the values are the higher the worse. More advanced techniques like ROAD (Rong et al. 2022) cannot be applied in this context, since the perturbation is applied uniformly over the entire image. In Table 8, we report the correlation between MaxSensitivity and human scores, outlining a non-significant correlation with the metric and some questions. Surprisingly, the most correlated questions are **Q1-4**, which are not requesting humans to assess the stability of the explanation, something instead partially addressed by **Q5** and **Q6**. However, the correlation is very weak anyway, questioning any further claims.

Complexity: As humans have an implicit tendency to favor simple alternatives when facing a comparison between different hypotheses, providing simple and compact explanations is vital for human-machine synergy (Cowan 2001). Alternative methods for estimating the *complexity* of an explanation are available, from simple above-threshold counting to more advanced information-theoretic techniques (Chalasan et al. 2020; Bhatt, Weller, and Moura 2021; Nguyen and Martínez 2020). To test whether those metrics are correlated to human scores, we report in Table 9 the correlation between human votes and Sparseness (Chalasan et al. 2020), which estimates explanation *complexity* as the Gini Index (Hurley and Rickard 2009) of the absolute values of the image attribution. The result is a metric value in the range $[0, 1]$, where higher values indicate more sparseness. The computation of the Gini index is detailed in Algorithm 2.

Algorithm 2: Pseudo code for Gini coefficient calculation from Hedström et al. (2023)

Require: Explanation e

```

1:  $array \leftarrow flatten(e)$ 
2:  $array \leftarrow |array|$  {Take absolute value}
3:  $array \leftarrow sort(array, ascending = True)$ 
4:  $index \leftarrow arange(1, array.shape[0] + 1)$ 
5:  $n \leftarrow array.shape[0]$ 
6: return  $\frac{\sum (2 \cdot index - n - 1) \cdot array}{n \cdot \sum array}$ 

```

We used the Quantus library (Hedström et al. 2023) for implementing the previous metrics, and we present the raw metric values in Table 10, aggregated by explainer and model. Overall, none of the above metrics exhibits a significant correlation with user scores.

B.3 Dataset analysis

To further explore annotator preferences, we identified the top-12 XAI techniques selected by each annotator and visualized the results in the histogram shown in Figure 16. Unlike Table 11, this analysis focuses on the top-12 techniques per annotator,

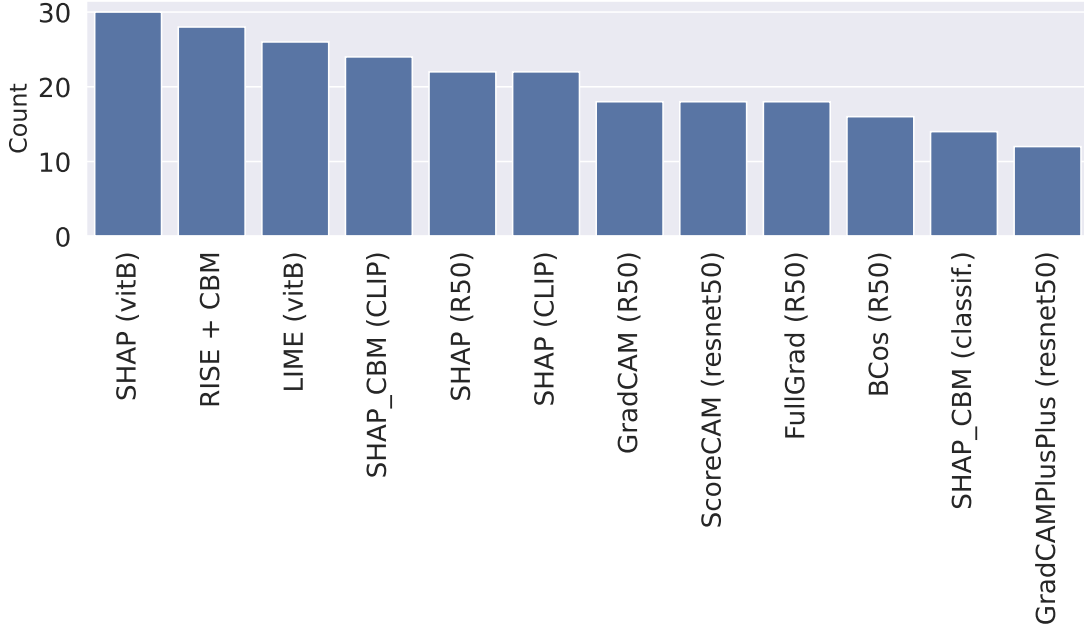


Figure 16: **Histogram showing the top-12 XAI techniques preferred by each annotator.**

removing the influence of votes among the top-12 techniques to reduce noise and better capture annotator preferences. From this figure, we observe that classical methods such as LIME and SHAP stand out as one of the most frequently preferred. This suggests a strong preference for well-established saliency-based methods. Additionally, there is a notable inclination towards methods that probe the model’s reaction to input perturbations. A distinct aspect is the inclusion of B-cos, which generates explanations through the incorporation of a dedicated layer, offering a unique mechanism compared to other perturbation-based techniques. Of the 11 most popular techniques among annotators, only two are based on CBMs, indicating a general preference for saliency maps over concept-based explanations.

Next, we aggregated the scores using majority voting and calculated QWC scores to measure the agreement between individual annotators and the aggregated score. We further analyzed the QWC scores by gender and age groups to assess any systematic differences in interpretation. As shown in Figure 17, the kappa scores indicate that there is generally consistent agreement across different age and sex groups, although older annotators show slightly less consistency. This highlights that while demographic factors may introduce some variation, they do not substantially impact the overall interpretability evaluation. Notable exceptions are observed for Q3 and Q4, which address the notions of objectivity and clarity. The decrease in agreement can be attributed to the increased subjectivity required by these questions compared to others.

In Table 11, we present the average mode of votes for each XAI technique. The primary observation is the challenge in discerning clear differences among XAI methods, largely attributable to their high sensitivity to the specific backbones to which they are applied. Regarding the differences among questions, we note significant similarities between Q1 and Q2, as well as between Q3 and Q4. It is particularly noteworthy that raters globally assessed explanations as clearer and more objective, with mean scores of 3.46 for Q3 and 3.44 for Q4, compared to their faithfulness to the model, which had mean scores of 2.83 for Q1 and 2.82 for Q2. Beyond confirming the multifaceted nature of human assessment, this underscores the difficulties encountered by current XAI methods in conveying the behavior of the model, rather than merely creating clear methods for displaying explanations.

C. PASTA-dataset: Extra questions

To enhance the study, we solicited responses from a subset of annotators (15 annotators) to address additional questions. These questions did not directly involve generated explanations. Instead, the questions focused on their overall perceptions of XAI and how they personally approach explanations. Consequently, this section aims to take a broader perspective and reflect more comprehensively from a user study viewpoint.

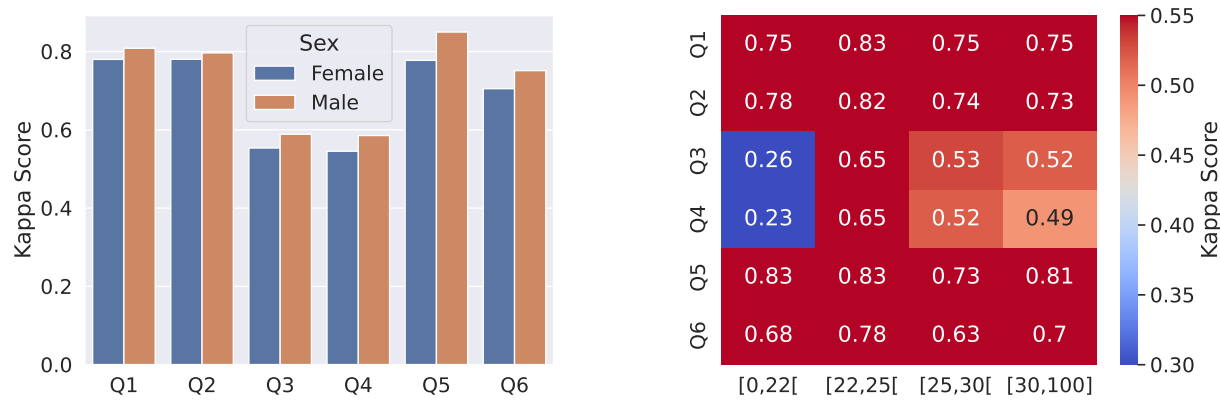


Figure 17: Cohen’s kappa statistics showing agreement between annotators, aggregated by sex and age groups.

C.1 Image labeling

For each image, participants had to explain what led them to classify the displayed image as the model’s prediction. Participants responded openly using a text form.

A first set of questions aims at having annotators establish a baseline, i.e., by interpreting and explaining what makes an image recognizable as a specific object or class. The process is constituted of these two questions:

- Q0.1: What part makes you classify this image as ****? (write an explanation extracting concepts)
- Q0.2: What part of the input helps the prediction? (draw bounding boxes on the image)

Similarly, they were asked to describe the elements of the image that helped them make the decision to classify the image as the model did. These two questions (Q0.1 and Q0.2) are used to establish a baseline for interpreting what makes an image recognizable as a specific object or class, and what are the salient features of the images that would explain this choice.

We investigated potential biases in the annotations themselves by examining the differences in how annotators approached CBM-based and saliency-based explanations. For CBM explanations, we focused on the text written by annotators in response to question Q0.1, assessing whether annotators preferred explanations that closely resembled their own textual responses. To quantify this, we transformed CBM explanations into text by concatenating the top concepts used in the explanation and calculated the BLEU (Papineni et al. 2002) and ROUGE scores (Lin 2004) between these explanations and the annotators’ text responses. As shown in Figure 18, the ROUGE score reveals a slight correlation between the explanations and the annotators’ expectations for questions Q1, Q2, Q3, and Q4. This suggests that annotators are inclined to favor explanations that align with their preconceived notions, potentially introducing a bias toward consistency with their initial answers.

Moreover, we observed that questions Q1, Q2, Q3, and Q4 exhibit high intercorrelation, as do questions Q5 and Q6. This clustering indicates that annotators tend to evaluate explanations similarly across these sets of questions, which may reflect underlying patterns in how different types of explanations are perceived.

For saliency-based explanations, we analyzed the bounding boxes provided by annotators in response to question Q0.2. We evaluated the correlation between various metrics and the annotators’ answers, including:

1. the total sum of pixel intensities in the saliency map (“SUM_all”),
2. the sum of pixel intensities within the area of the image identified by the bounding box (“SUM_pos”),
3. the sum of pixel intensities outside the bounding box (“SUM_neg”),
4. the entropy of the saliency map (“Entropy”).

Figure 18 shows that questions Q1, Q2, Q3, and Q4 are highly correlated with each other, as are questions Q5 and Q6. Additionally, all metrics except for “SUM_pos” show some correlation with questions Q1–Q4. This suggests that annotators may focus heavily on background features and salient objects when answering these questions, potentially overlooking finer details in the bounding box area.

Overall, these analyses highlight several potential biases in the dataset. Annotators exhibit a preference for certain types of explanations, particularly saliency maps, and tend to favor explanations that align with their expectations, as evidenced by the correlation between their text responses and the explanations. Additionally, while demographic factors such as age and gender do not significantly impact the overall evaluation, the slight decrease in consistency among older annotators warrants further investigation. The study involved 15 annotators, all from the same cultural background, which may introduce some shared perspectives or biases. To mitigate this, future studies could benefit from a more diverse group of annotators.

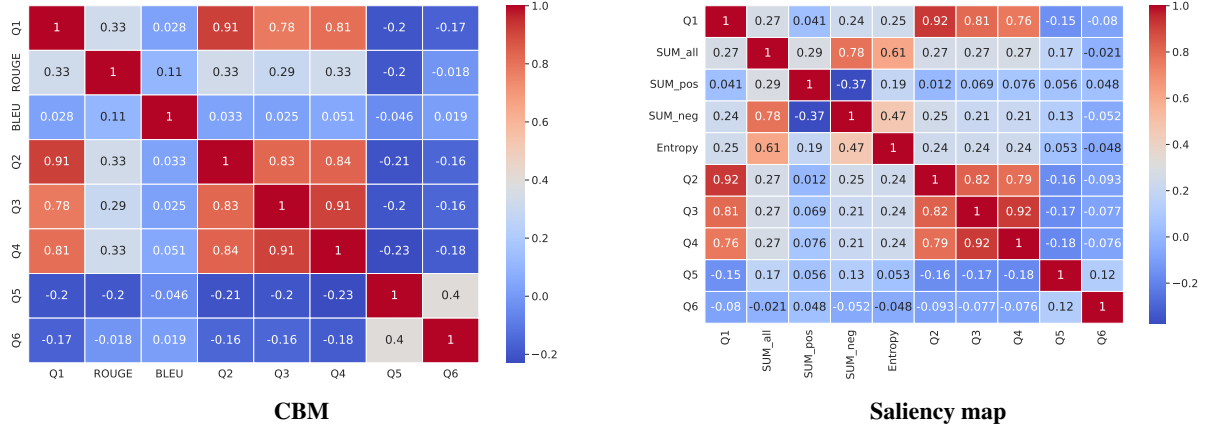


Figure 18: **Correlation between the various questions and key metrics for saliency and CBM explanations.** For CBM, the criteria used are the BLEU (Papineni et al. 2002) and ROUGE scores (Lin 2004) scores between the explanation and the text from question Q0.1. For saliency maps, the metrics include the total pixel sum (SUM_all), the sum of pixels within the annotator-provided bounding box (SUM_pos) from question Q0.2, the sum of pixels outside the bounding box (SUM_neg), and the entropy of the saliency map (Entropy).

C.2 Desiratas ranking

After the annotation process is completed, evaluators are presented with a set of questions assessing their stance on the questions asked.

In addition to annotating the samples that comprise the PASTA-dataset, each participant in the study was asked to respond to the following questions:

- Q7: Could you rank the different qualities of the explanation in order of importance? *Expectedness, Trustworthiness, Complexity, Robustness, Objectivity.*
- Q8: Can you please order the different questions from Q1, Q2, Q3, Q4, Q5, and Q6 from the less important to the more important questions to assess the quality of the explanation?
- Q9: Can you please order the different questions from Q1, Q2, Q3, Q4, Q5 and Q6 from the most difficult to the easiest?

The results for Q7 are presented in Table 12. The data indicate that evaluators place a higher value on Trustworthiness and Complexity, while Objectivity is ranked significantly lower. This finding aligns with the work of Liao et al. (2022), who asked a similar question but focused on a pool of experts.

Table 13 summarizes the results for Q8 and Q9. According to user feedback, Q1 is deemed the most important question. Notably, there is a strong correlation between the responses to Q8 and Q9: the questions perceived as easiest to answer are also regarded as the most important. Interestingly, there is a low correlation between the importance assigned to each question and the axioms they represent, highlighting a distinction between the perception of an axiom and the execution of the associated task. Furthermore, both Q8 and Q9 reveal a separation in ranking among Q1 to Q4 and Q5 and Q6, which resonates with the dataset analysis.

D. PASTA-score: Implementation details

D.1 Technical information

Hyperparameters In all experiments, we employed the Adam optimizer (Kingma and Ba 2017) with a batch size of 256, training for 600 epochs at a learning rate of 2×10^{-6} . Additionally, we configured the parameters as follows: α was set to 1, β to 0.001, and γ to 0.01. We also applied a weight decay of 1×10^{-6} . The model utilized a hidden layer size of [512, 64]. For concept-based explanations, we used the top 15 concepts, with no template. For Q3 to Q6, we excluded a part of the annotations related to COCO, due to a presence of outliers.

Regarding the division between the training, validation, and test sets, we imposed restrictions on the selected samples to ensure no overlap in XAI methods or images on which the explanations are based, thereby preventing overfitting. To achieve this, we proceeded as follows. First, we assigned an ID to each of the images (IMG_ID) and each of the XAI methods (XAI_ID). As mentioned in the dataset specifications, $\text{IMG_ID} \in [1; 1000]$ and $\text{XAI_ID} \in [1; 46]$. Secondly, given these sets and a seed, we randomly selected 70% of the XAI_ID and 70% of the IMG_ID. Thirdly, we included in the training set only those samples that presented both a valid XAI_ID and IMG_ID ($\neg((\text{XAI_ID_train} = \text{XAI_ID_test}) \vee (\text{IMG_ID_train} = \text{IMG_ID_test}))$). We

followed the same procedure with the remaining set to construct the validation and test sets. All remaining samples were discarded for the run.

Evaluation metrics The quadratic weighted Cohen’s Kappa (QWK) measures inter-rater agreement, adjusting for chance and penalizing disagreement based on its magnitude. The formula is:

$$\text{QWK} = \frac{\sum_{i,j} w_{ij} O_{ij} - \sum_{i,j} w_{ij} E_{ij}}{1 - \sum_{i,j} w_{ij} E_{ij}}, \quad (7)$$

where:

- O_{ij} and E_{ij} are the observed and expected frequencies, respectively.
- $w_{ij} = 1 - \frac{(i-j)^2}{(k-1)^2}$ is the quadratic weight for categories i and j .

The Mean Squared Error (MSE) measures the average squared difference between predicted and actual values. It is given by:

$$\text{MSE} = \frac{1}{N_s} \sum_{k=1}^{N_s} (m_k - \hat{m}_k)^2. \quad (8)$$

The Spearman Correlation Coefficient (SCC) measures the rank correlation between two variables. It is calculated using the ranks of the data points and is given by:

$$\text{SCC} = 1 - \frac{6 \sum_i d_i^2}{N_s(N_s^2 - 1)}, \quad (9)$$

where d_i is the difference between the ranks of each pair of values.

Loss Functions Here, we define the three losses used to train our PASTA-model.

The Cosine Similarity Loss measures the cosine similarity between the predicted explanations scores \hat{m}_k and the ground truth explanations scores m_k , ensuring alignment in their direction:

$$L_s = 1 - \frac{\sum_{k=1}^{N_s} \hat{m}_k m_k}{\sqrt{\sum_{k=1}^{N_s} \hat{m}_k^2} \sqrt{\sum_{k=1}^{N_s} m_k^2}} \quad (10)$$

The Mean Squared Error (MSE) loss measures the squared difference between predicted and true explanations, penalizing larger errors more heavily:

$$L_{mse} = \frac{1}{N_s} \sum_{k=1}^{N_s} (\hat{m}_k - m_k)^2 \quad (11)$$

This Ranking Loss ensures the correct ranking of explanations by penalizing cases where the predicted ranking contradicts the true ranking:

$$L_r = \frac{1}{\hat{N}_s} \sum_{k_1, k_2} \max(0, -(\hat{m}_{k_1} - \hat{m}_{k_2})(m_{k_1} - m_{k_2})) \quad (12)$$

Here, \hat{N}_s represents the total number of pairs considered for the ranking loss.

Computational resources The experiments were conducted using a V100-32GB GPU. The training and inference times are summarized in Table 14. It is important to note that, for both inference and testing, the majority of the computational time is dedicated to precomputing VLM embeddings, as the scoring network itself is relatively lightweight and requires minimal computational resources.

D.2 Ablation studies

Aggregation of the votes

Formulas In the dataset, we have access to 5 votes per question. Then, if we denote the set of votes as $\{m_i^j[a]\}_{a=1}^{N_a}$, where $N_a = 5$ is the number of annotations:

$$\text{Mode}(m_i^j) = \arg \max_a \text{Count}(m_i^j[a]), \quad (13)$$

where $\text{Count}(m_i^j[a])$ represents the frequency of each vote a in the set.

Given the subjective nature of the annotations and the presence of multiple responses to the same question (five answers per question), we explored different methods for determining the ground truth. In Table 15, we tested how PASTA-score training is affected when using the mean, mode, or median as the ground truth. Since this parameter significantly impacts the dispersion of the samples, it is not surprising that the results vary, particularly when using the mean. However, in all our experiments, we opted to use the mode, as phenomena of high non-consensus were observed.

Add of label information in the PASTA-score embedding. In the current iteration of the PASTA-score, information regarding the predicted class is integrated into the embeddings supplied to the scoring network. Specifically, each predicted label is encoded as a one-hot vector and concatenated with the embedding. In this study, we aim to measure the impact of this design choice by comparing it with an alternative approach that utilizes only embeddings as input to the scoring network.

As illustrated in Table 16, the integration of label information exhibits a positive influence, aligning with the hypothesis that such contextual data enhances the comprehension of human behavior patterns affecting ratings. However, the observed improvement is modest. This phenomenon can be attributed to several factors, including the extensive number of labels employed across the datasets (26), which is commensurate with the quantity of unique images. As a result, the inclusion of label information may introduce redundancy or lead to overfitting, thereby influencing the efficiency of the scoring mechanism.

Scoring functions In this section, we examine the influence of various scoring network architectures on performance. Specifically, we tested alternatives such as Ridge Regression, Lasso Regression, Support Vector Machines. The results of these experiments are presented in Table 17.

By analyzing the performance of the different scoring functions, we observe that PASTA, implemented with a multi linear perceptron and leveraging the loss functions described in Section , achieves superior results in terms of the Quadratic Weighted Kappa score and Spearman Correlation Coefficient. These outcomes highlight its effectiveness in accurately ranking labels. However, SVM exhibit lower Mean Square Error, suggesting better numerical precision in predicting label values. Our primary objective is to develop a robust metric for ranking XAI methods. As such, we place greater emphasis on metrics that assess ranking accuracy. Based on this criterion, the PASTA framework is favored over alternative scoring networks due to its superior performance in rank-oriented evaluations.

Explanation embeddings

This section presents several ablation studies that informed the development of our current methodology for embedding explanations. Throughout these experiments, the Siglip model was utilized as the VLM encoder.

Saliency Regarding saliency-based explanations, a key question arises about what should be considered as the image representing the explanation. Two variants were considered: using the heatmap visualization that is presented to users, as shown in Equation 1, or the input image as defined as:

$$\phi_{\text{image}}(e_i^j) = \text{VLM}_{\text{image}}(x_i \times e_i^j) \quad (14)$$

The element-wise multiplication of the input image with the saliency map selectively blurs the image, with regions corresponding to lower activation values being blurred, while areas with higher activation values remain clear.

The results are presented in Table 18, where a slight improvement is observed in favor of using the image as a heatmap. This can be attributed to the fact that, despite being more computationally ambiguous, the heatmap display reveals the entire image. Additionally, this representation closely resembles the format of the samples provided to annotators.

CBM Concerning concept bottleneck explanation, which basically can be interpreted as a dictionary attributing a scalar for each concept. One crucial step is converting CBM activations to VLM embeddings. We tested two ways to do so:

- By considering the raw text of concepts, ordered by importance (Equation 2)
- By using a sum of all the VLM embeddings of text, weighted by its activations:

$$\phi_{\text{text}}(e_i^j) = \frac{1}{\|e_i^j\|} \sum_k^{N_k} e_i^j[k] \text{VLM}_{\text{text}}(\text{concept}_i[k]) \quad (15)$$

If we use the first solution, there are questions about the number of concepts to keep, that we note as the parameters N_{top} . Table 19 presents the influence of N_{top} while 20 presents the influence of different ways to compute the embeddings. Analysis of the results indicates that an adequate number of concepts enhances ranking performance, which eventually plateaus, thereby informing the selection of $N_{\text{top}} = 15$. Regarding the embedding procedure, optimal outcomes were achieved by encoding the top concepts as a sentence. The inclusion of a template demonstrated negligible influence on overall performance metrics.

E. PASTA-score: Additional Examples

Table 10: **Raw metric values averaged for each explainer and model.** Each value is the average result on 5 runs with the standard deviation.

Saliency Method	Model	Faithfulness (ROAD)	Robustness (Gaussian noise)	Sparseness
GradCAM	resnet50	0.12 ± 0.20	0.92 ± 0.35	0.65 ± 0.11
GradCAM	vitB	0.02 ± 0.03	1.65 ± 1.77	0.50 ± 0.26
AblationCAM	vitB	0.02 ± 0.03	1.51 ± 1.19	0.74 ± 0.21
AblationCAM	CLIP-zero-shot	0.02 ± 0.02	1.39 ± 0.70	0.79 ± 0.16
EigenCAM	resnet50	0.12 ± 0.21	0.93 ± 0.47	0.79 ± 0.07
EigenCAM	vitB	0.02 ± 0.03	1.03 ± 0.33	0.58 ± 0.06
EigenCAM	CLIP-zero-shot	0.02 ± 0.02	0.78 ± 0.38	0.56 ± 0.09
EigenGradCAM	resnet50	0.12 ± 0.20	0.96 ± 0.57	0.78 ± 0.07
EigenGradCAM	vitB	0.02 ± 0.03	2.40 ± 1.74	0.83 ± 0.19
EigenGradCAM	CLIP-zero-shot	0.02 ± 0.03	1.26 ± 0.61	0.72 ± 0.14
FullGrad	resnet50	0.11 ± 0.19	0.48 ± 0.15	0.40 ± 0.06
FullGrad	vitB	0.02 ± 0.02	1.08 ± 0.48	0.38 ± 0.06
GradCAM	CLIP-zero-shot	0.02 ± 0.02	1.21 ± 0.66	0.57 ± 0.17
GradCAMPlusPlus	resnet50	0.12 ± 0.20	0.71 ± 0.26	0.60 ± 0.10
GradCAMPlusPlus	vitB	0.02 ± 0.02	2.33 ± 2.17	0.59 ± 0.28
GradCAMPlusPlus	CLIP-zero-shot	0.02 ± 0.02	1.46 ± 0.93	0.63 ± 0.24
GradCAMElementWise	resnet50	0.11 ± 0.20	0.72 ± 0.25	0.58 ± 0.10
GradCAMElementWise	vitB	0.02 ± 0.02	1.20 ± 0.40	0.59 ± 0.09
GradCAMElementWise	CLIP-zero-shot	0.02 ± 0.02	0.71 ± 0.28	0.38 ± 0.08
HiResCAM	resnet50	0.12 ± 0.20	0.91 ± 0.35	0.65 ± 0.11
HiResCAM	vitB	0.02 ± 0.03	1.92 ± 1.13	0.71 ± 0.24
HiResCAM	CLIP-zero-shot	0.02 ± 0.02	1.43 ± 0.49	0.69 ± 0.13
LIME	resnet50	0.15 ± 0.22	0.49 ± 0.06	0.12 ± 0.04
ScoreCAM	resnet50	0.12 ± 0.21	0.78 ± 0.31	0.59 ± 0.10
ScoreCAM	vitB	0.02 ± 0.03	1.22 ± 0.65	0.53 ± 0.18
XGradCAM	resnet50	0.12 ± 0.20	0.88 ± 0.34	0.65 ± 0.11
XGradCAM	vitB	0.02 ± 0.03	1.37 ± 0.30	0.62 ± 0.07
XGradCAM	CLIP-zero-shot	0.02 ± 0.02	1.30 ± 0.20	0.59 ± 0.06
DeepFeatureFactorization	resnet50	0.11 ± 0.18	0.95 ± 0.52	0.34 ± 0.12
DeepFeatureFactorization	vitB	0.02 ± 0.03	0.63 ± 0.23	0.28 ± 0.05
DeepFeatureFactorization	CLIP-zero-shot	0.02 ± 0.03	0.65 ± 0.31	0.33 ± 0.08
LIME	vitB	0.02 ± 0.03	0.50 ± 0.05	0.15 ± 0.03
BCos	resnet50-bcos	0.15 ± 0.24	0.88 ± 0.31	0.50 ± 0.09
LIME	CLIP-zero-shot	0.02 ± 0.03	0.58 ± 0.09	0.16 ± 0.05
SHAP	resnet50	0.13 ± 0.21	1.37 ± 0.46	0.50 ± 0.10
SHAP	vitB	0.02 ± 0.03	1.05 ± 0.45	0.40 ± 0.09
SHAP	CLIP-zero-shot	0.02 ± 0.03	1.19 ± 0.38	0.46 ± 0.10
AblationCAM	resnet50	0.12 ± 0.19	1.44 ± 0.48	0.71 ± 0.11

Table 11: XAI techniques with aggregated scores across different evaluation metrics.

XAI Technique	Q1	Q2	Q3	Q4	Q5	Q6
GradCAM (ResNet50)	3.22	3.22	3.67	3.66	2.22	4.65
GradCAM (ViT-B)	2.63	2.64	3.41	3.41	2.53	4.62
GradCAM (CLIP-zero-shot)	2.40	2.40	3.30	3.29	2.63	4.79
LIME (ResNet50)	2.51	2.49	3.21	3.20	3.78	4.51
LIME (ViT-B)	3.00	2.98	3.55	3.53	3.23	4.53
LIME (CLIP-zero-shot)	2.75	2.74	3.35	3.33	3.61	4.53
SHAP (ResNet50)	3.00	2.99	3.50	3.49	2.64	4.70
SHAP (ViT-B)	3.10	3.09	3.58	3.55	2.57	4.70
SHAP (CLIP-zero-shot)	3.14	3.13	3.55	3.52	2.64	4.68
AblationCAM (ResNet50)	2.71	2.70	3.46	3.46	3.07	4.17
AblationCAM (ViT-B)	2.29	2.28	3.21	3.21	2.48	4.66
AblationCAM (CLIP-zero-shot)	2.03	2.03	2.99	3.00	2.34	4.64
EigenCAM (ResNet50)	3.12	3.11	3.65	3.63	2.26	4.25
EigenCAM (ViT-B)	3.13	3.13	3.65	3.63	2.27	4.29
EigenCAM (CLIP-zero-shot)	3.27	3.28	3.81	3.76	1.98	4.11
EigenGradCAM (ResNet50)	3.09	3.09	3.61	3.60	2.13	4.32
EigenGradCAM (ViT-B)	2.00	2.00	2.90	2.90	2.98	4.69
EigenGradCAM (CLIP-zero-shot)	2.73	2.73	3.45	3.43	2.62	4.58
FullGrad (ResNet50)	3.50	3.49	3.86	3.80	1.98	4.03
FullGrad (ViT-B)	2.28	2.27	3.16	3.16	3.13	4.64
GradCAMPlusPlus (ResNet50)	3.26	3.26	3.73	3.69	2.20	4.38
GradCAMPlusPlus (ViT-B)	2.58	2.58	3.33	3.31	3.10	4.69
GradCAMPlusPlus (CLIP-zero-shot)	2.31	2.31	3.27	3.26	2.78	4.79
GradCAMElementWise (ResNet50)	3.23	3.22	3.69	3.67	2.19	4.32
GradCAMElementWise (ViT-B)	2.12	2.12	2.95	2.97	2.69	4.65
GradCAMElementWise (CLIP-zero-shot)	3.10	3.10	3.64	3.61	2.25	4.37
HiResCAM (ResNet50)	3.28	3.27	3.72	3.69	2.21	4.60
HiResCAM (ViT-B)	2.03	2.03	2.98	2.98	2.93	4.80
HiResCAM (CLIP-zero-shot)	2.38	2.38	3.21	3.21	2.73	4.80
ScoreCAM (ResNet50)	3.32	3.32	3.73	3.70	2.32	4.50
ScoreCAM (ViT-B)	3.19	3.18	3.73	3.68	2.44	4.66
XGradCAM (ResNet50)	3.26	3.27	3.71	3.69	2.10	4.63
XGradCAM (ViT-B)	2.37	2.37	3.29	3.28	3.78	4.65
XGradCAM (CLIP-zero-shot)	2.59	2.59	3.46	3.45	3.88	4.70
DeepFeatureFactorization (ResNet50)	3.41	3.41	3.86	3.82	2.22	4.18
DeepFeatureFactorization (ViT-B)	3.03	3.02	3.72	3.68	2.18	4.26
DeepFeatureFactorization (CLIP-zero-shot)	3.22	3.22	3.78	3.72	2.02	4.07
CLIP-QDA-sample	2.20	2.19	3.11	3.09	2.72	4.70
CLIP-Linear-sample	3.10	3.08	3.48	3.45	1.68	4.46
LIME_CBM (CLIP-QDA)	2.69	2.69	3.38	3.36	3.64	4.59
SHAP_CBM (CLIP-QDA)	3.09	3.08	3.53	3.52	2.82	4.54
LIME_CBM (CBM-classifier-logistic)	2.90	2.88	3.38	3.35	2.77	4.49
SHAP_CBM (CBM-classifier-logistic)	3.08	3.06	3.46	3.43	2.43	4.30
Xnesyl-Linear	2.36	2.34	3.22	3.19	2.45	3.83
BCos (ResNet50-BCos)	2.86	2.85	3.49	3.46	2.30	3.84
RISE-CBM (CBM-classifier-logistic)	3.28	3.27	3.66	3.62	2.22	4.35

Table 12: **Average positions of axioms for question 7.** Lower rankings indicate that the axiom is considered more important by evaluators, while higher rankings suggest the axiom is considered less important. Results sorted by ascending order.

<i>Axiom</i>	<i>Average Position (Q7) ↓</i>
<i>Trustworthiness</i>	2.47 ± 1.48
<i>Complexity</i>	2.53 ± 1.58
<i>Robustness</i>	2.97 ± 1.06
<i>Expectedness</i>	3.20 ± 1.05
<i>Objectivity</i>	3.77 ± 1.36

Table 13: **Average positions of questions 1 to 6 for Q8 and Q9.** For Q8, higher rankings indicate that the question is considered more important by evaluators, while lower rankings suggest the question is considered less important. For Q9, lower rankings indicate that the question is considered more difficult to evaluate, while lower rankings suggest the question is considered less difficult.

<i>Question</i>	<i>Average Position (Q8) ↑</i>	<i>Average Position (Q9) ↓</i>
Q1	4.10 ± 1.32	4.00 ± 1.21
Q2	3.90 ± 1.29	4.23 ± 1.35
Q3	4.03 ± 1.77	4.53 ± 1.70
Q4	3.13 ± 1.41	3.67 ± 1.40
Q5	2.63 ± 1.66	1.80 ± 0.57
Q6	3.00 ± 1.95	2.54 ± 1.72

Table 14: **Training and Inference Times on GPU and CPU.** Results for the PASTA-score^{SIGLIP} variant.

<i>Device</i>	<i>Training Time (s)</i>	<i>Inference Time (s)</i>
GPU	1048.74	36.12
CPU	10035.98	796.41

Table 15: **Comparison of the influence of ground truth generation methods.** Each value is the average result on 5 runs with the standard deviation.

<i>Label Type</i>	<i>MSE</i>	<i>QWK</i>	<i>SCC</i>
Mode	0.989 ± 0.113	0.471 ± 0.055	0.501 ± 0.052
Mean	0.774 ± 0.067	0.506 ± 0.049	0.532 ± 0.043
Median	0.924 ± 0.093	0.479 ± 0.052	0.509 ± 0.046

Table 16: **Impact of Adding Labels to the Encodings.** Each value is the average result on 5 runs with the standard deviation.

<i>Computation</i>	<i>MSE</i>	<i>QWK</i>	<i>SCC</i>
<i>Embeddings</i>	0.987 ± 0.098	0.469 ± 0.047	0.497 ± 0.045
<i>Embeddings + Labels</i>	0.989 ± 0.113	0.471 ± 0.055	0.501 ± 0.052

Table 17: **Impact of the Scoring Function.** Each value is the average result on 5 runs with the standard deviation.

<i>Scoring Function</i>	<i>MSE</i>	<i>QWK</i>	<i>SCC</i>
<i>PASTA</i>	0.989 ± 0.113	0.471 ± 0.055	0.501 ± 0.052
<i>SVM</i>	0.965 ± 0.077	0.463 ± 0.056	0.501 ± 0.051
<i>Ridge</i>	1.169 ± 0.143	0.423 ± 0.046	0.444 ± 0.043
<i>Lasso</i>	0.998 ± 0.075	0.395 ± 0.048	0.454 ± 0.052

Table 18: **Influence of the saliency computation process.** *Heatmap* refers to the process defined in Equation 1 and *Masked image* refers to the process defined in Equation 14. Each value is the average result on 5 runs with the standard deviation.

<i>Embedded Image</i>	<i>MSE</i>	<i>QWK</i>	<i>SCC</i>
<i>Heatmap</i>	0.989 \pm 0.113	0.471 \pm 0.055	0.501 \pm 0.052
<i>Blur</i>	0.992 \pm 0.089	0.470 \pm 0.048	0.498 \pm 0.043

Table 19: **Influence of the number of words selected as an input text N_{top} .** Each value is the average result on 5 runs with the standard deviation.

N_{top}	<i>MSE</i>	<i>QWK</i>	<i>SCC</i>
5	0.988 \pm 0.101	0.466 \pm 0.047	0.495 \pm 0.043
10	0.992 \pm 0.115	0.461 \pm 0.066	0.493 \pm 0.057
15	0.989 \pm 0.113	0.471 \pm 0.055	0.501 \pm 0.052
20	0.994 \pm 0.122	0.470 \pm 0.059	0.498 \pm 0.056

Table 20: **Influence of the CBM explanation embedding process.** *Weightened* refers to the process described in Equation 15, *Sentence* refers to the process described in Equation 2, preceded with the template noted in *Template*. Each value is the average result on 5 runs with the standard deviation.

<i>Computation</i>	<i>MSE</i>	<i>QWK</i>	<i>SCC</i>	<i>Template</i>
<i>Weighted</i>	1.212 \pm 0.288	0.392 \pm 0.077	0.425 \pm 0.082	“ ”
<i>Sentence</i>	0.989 \pm 0.113	0.471 \pm 0.055	0.501 \pm 0.052	“ ”
<i>Sentence</i>	0.986 \pm 0.119	0.469 \pm 0.061	0.504 \pm 0.055	“Concepts in explanation:”

Table 21: **PASTA scores corresponding to different explanations.** Dataset: catsdogscars. Label: dog




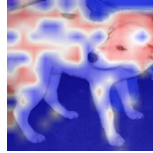


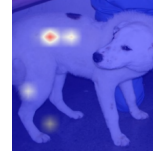
							
P (Q1)	2.01	2.04	3.94	3.01	3.81	3.97	2.14
P (Q2)	1.90	1.82	3.31	2.80	3.57	3.37	1.70
P (Q3)	2.93	2.58	3.65	4.06	4.02	3.65	2.83
P (Q4)	3.04	2.95	3.84	4.09	4.14	3.84	2.75

Table 22: **PASTA scores corresponding to different explanations.** Dataset: MonumAI. Label: Baroque

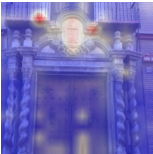
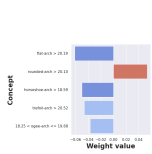


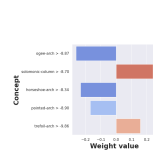
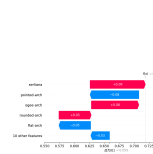

							
P (Q1)	2.45	1.01	3.06	4.00	1.00	1.67	3.22
P (Q2)	2.51	1.26	2.99	3.48	1.57	1.52	3.51
P (Q3)	3.67	1.52	3.51	3.71	2.05	1.54	3.69
P (Q4)	3.35	1.33	3.45	3.89	1.33	1.59	3.79

Table 23: **PASTA scores corresponding to different explanations.** Dataset: COCO. Label: transportation

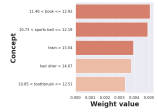



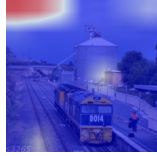


							
P (Q1)	1.21	3.24	2.46	3.44	2.01	2.80	2.40
P (Q2)	1.61	3.22	2.45	3.36	2.23	2.75	2.37
P (Q3)	1.43	3.94	3.45	3.78	3.01	3.69	3.41
P (Q4)	1.59	3.65	3.20	3.50	2.96	3.25	3.28

Table 24: **PASTA scores corresponding to different explanations.** Dataset: PascalPart. Label: cat


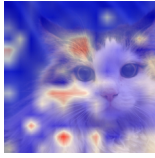
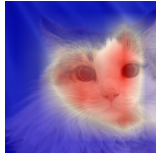

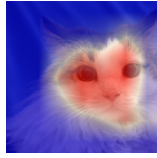
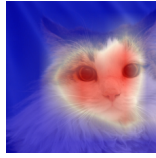
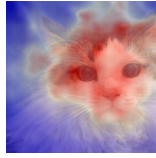
							
P (Q1)	2.02	1.68	3.90	2.51	3.93	2.50	3.30
P (Q2)	2.53	1.71	3.91	2.55	3.90	2.60	3.42
P (Q3)	2.88	2.77	3.78	3.22	3.94	3.30	3.80
P (Q4)	3.06	2.82	3.78	3.27	3.82	3.26	3.82

Table 25: **PASTA scores corresponding to different explanations.** Dataset: PascalPart. Label: person

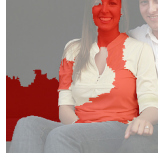

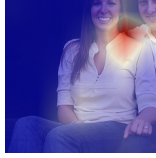
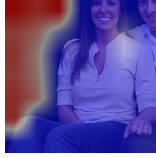
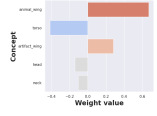
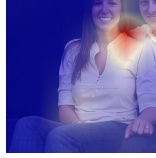
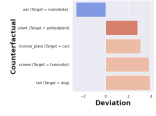
							
P (Q1)	3.68	3.55	3.69	3.12	1.35	3.71	1.93
P (Q2)	3.46	3.19	3.16	3.07	1.74	3.16	1.81
P (Q3)	3.50	3.64	3.64	3.02	1.77	3.59	2.56
P (Q4)	4.23	4.09	4.05	3.82	1.29	4.04	1.91

Table 26: **PASTA scores corresponding to different explanations.** Dataset: COCO. Label: cultural




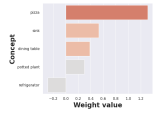
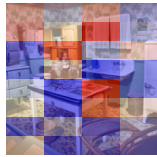

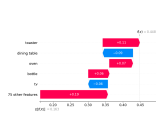
							
P (Q1)	2.65	2.27	2.78	1.21	2.96	2.75	1.45
P (Q2)	2.21	1.73	2.31	1.64	2.82	2.14	1.83
P (Q3)	2.40	2.17	3.05	1.37	3.25	2.49	1.72
P (Q4)	2.49	2.20	2.84	1.30	3.06	2.75	1.92

Table 27: **PASTA scores corresponding to different explanations.** Dataset: catsdogscars. Label: car





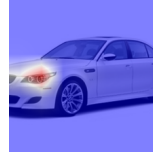

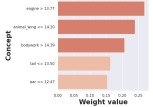
							
P (Q1)	3.20	2.67	4.80	2.10	2.74	4.80	1.50
P (Q2)	3.18	2.60	4.69	1.53	2.37	4.69	1.64
P (Q3)	2.98	2.54	4.30	2.55	3.17	4.30	2.16
P (Q4)	3.34	2.47	4.06	2.51	3.01	4.06	1.72

Table 28: **PASTA scores corresponding to different explanations.** Dataset: PascalPart. Label: motorbike

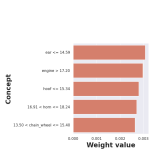
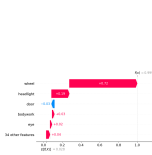


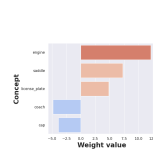
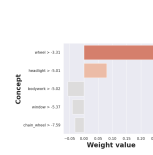

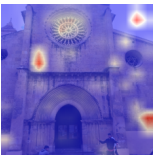



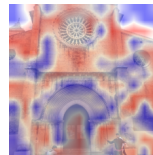

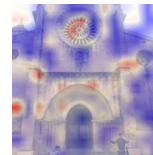
							
P (Q1)	1.26	1.42	3.38	2.43	1.10	1.00	3.26
P (Q2)	1.59	1.61	3.35	2.22	1.46	1.52	3.07
P (Q3)	2.18	1.43	4.41	3.31	1.96	1.77	4.18
P (Q4)	2.15	2.10	4.22	3.47	1.45	2.24	4.08

Table 29: **PASTA scores corresponding to different explanations.** Dataset: MonumAI. Label: Gothic

							
P (Q1)	2.74	3.75	3.38	3.00	3.97	2.88	3.69
P (Q2)	2.51	3.43	3.13	2.86	3.91	2.79	3.44
P (Q3)	3.21	3.90	3.58	3.43	4.37	3.70	3.98
P (Q4)	3.18	3.85	3.51	3.38	4.25	3.52	3.84